NMP3-CT-2005-013998

PREDFIRE-NANO

Predicting Fire Behaviour of Nanocomposites from Intrinsic Properties

Specific Targeted Project
NMP research area(s)-
3.4.2.3 – 1 Materials by design: Bio-inspired materials and organic/inorganic hybrid materials.
3.4.2.1 – 2 Modelling and design of multi-functioned materials.
3.4.3.3 – 2 New life-cycle optimised, safety and environmental technologies for industrial production.

FINAL ACTIVITY REPORT

1st February 2005 to 31st December 2008

Date of Preparation: 31 March 2009

Start date of project: 1st February 2005
Duration: 3 years (extended by 11 months)
Project Coordinator: Prof M Delichatsios
University of Ulster
Project Coordinator: Professor Michael Delichatsios

TABLE OF CONTENTS FINAL REPORT

THIRD YEAR PERIODIC REPORT

1. EXECUTIVE SUMMARY: PROJECT DESCRIPTION, OBJECTIVES AND MAJOR RESULTS

1.1 The Consortium and overview of the project

The PREDFIRE project is supported as a Specific Targeted Research project under FP6 priority 3, Nanotechnologies and nano-sciences, knowledge-based multifunctional materials and new production processes and devices. The project is coordinated by the University of Ulster. Michael Delichatsios, Professor of Fire Dynamics and Flammability and acting director at FireSERT (the Institute for Fire Safety Engineering Research and Technology) is responsible for the overall coordination and will direct the research at UU. The project consortium comprises the following partners:

- University of Ulster, UK (Coordinator)
- University of Bolton, UK
- University of Edinburgh, UK
- CDCMP, Center for Plastics Engineering, Italy
- Ecole Nationale Supérieure de Chimie de Lille, France
- Minelco Specialities Ltd, UK
- Clariant GmbH, Germany
- Kabelwerk-Eupen, Germany
- Fire and Environment Protection Service, Germany
- IRIS Vernici s.r.l., Italy
- TOLSA SA, Spain
- Essexford Joinery Works Ltd, Ireland
- FIRE RAS Lab of Spectroscopy and Millimetre Wave Measurements, Russia

The overall aim of this STREP project is to develop a tool for the prediction of large-scale burning behaviour of polymer nanocomposites using intrinsic property data extracted from small-scale measurements. The focus is both on identifying the key intrinsic properties of these materials needed for predicting their fire behaviour and on relating their dependence on the physical and chemical structure of the material by specifically probing the morphology and nanodispersion of nanoparticles. Thus, this project will advance the knowledge in the frontier areas of nanotechnology and fire prediction and moreover, it will enable the rapid development of fire safe materials by providing the knowledge to design fire-safe polymer nanocomposites. This project is unique because it brings together fire retardant and fire engineering expertise for the first time, allowing intelligent approaches to polymer flammability to be applied to the problem of measuring nanocomposite flammability. The participants involved in this project represent the best combination of experts available in the world.

This project is developing a methodology to predict the real-scale burning behaviour of polymer nanocomposites from their intrinsic material properties. The development and availability of new fire retardant polymers over the last ten years has been driven by;

(a) the abandonment of halogen based fire retardants due to regulations,
(b) the growth of nanotechnology,
(c) the application of performance based fire safety engineering and
(d) the adoption of European harmonizing tests such as the SBI (Single Burning Item).

Especially promising for their fire retardancy has been the discovery of nanocomposites (nanoclay), which have distinct advantages over traditional fire retardants in production, amount of additive (only 2-5% compared to 20-70%) and recycling (simple clays). In addition, concurrent work (FP 6 NANOFIRE project, coordinated by Prof. Camino, CDCMP) investigates the use of traditional fire retardants together with nanocomposites to enhance the fire retardancy by promoting char formation during decomposition and thus, reducing the gases that can burn in the fire.

Serious impediments to the development of these materials are the absence of a fundamental methodology and tests to accurately and correctly assess their flammability and burning behaviour in fires. Standards approval tests (such as the limited oxygen index LOI and UL94), that were accepted for halogenated fire retardant polymers, are not capable of realistically assessing the fire behaviour of polymer nanocomposites (or even the large scale behaviour of halogenated fire retardant polymers, e.g. cables).
On the other hand, small-scale fundamental experiments (such as thermogravimetric analysis (TGA), differential scanning calorimetry (DSC) which measures the decomposition kinetics and energetics and FTIR (Fourier Transform Infrared spectroscopy)) are not sufficient to predict the fire behaviour of the materials. This work will combine measurements in these small scale apparatus and measurements in intermediate apparatus (the standard cone calorimeter or the Universal Flammability Apparatus (UFA)) to identify key properties of the pyrolysis chemistry that underpin the fire behaviour of the materials. It has been shown that measurements (at various heat fluxes on the material) in the UFA can provide effective global flammability (i.e. thermal, ignition and pyrolysis) properties that predict the *fire growth* behaviour of the simple, non-composite materials in real fires). However, further work proposed here will provide the properties needed to predict the burning behaviour and emission *of smoke and toxic products* from nanocomposite materials in real fires.
The project has been extended in 2007 by an additional partner (WP8) from Russia (FIRE RAS Lab of Spectroscopy and Millimetre Wave Measurements) with work related to a) examining the monodispersity of nanocmposite polymers by measuring their dielectric properties through mm wave radiation and b) measuring surface temperature by reflection of mm wave radiation.
The work and the budget for which Swintex was responsible was reassigned to CDCMP and ENSCL with the approval of eth commission.

Project objectives

This project has developed a methodology for the evaluation of flammability and safe design of fire materials. To achieve this aim, the plan was to :
a) Relate the intrinsic flammability properties to the nanodispersion of the base material modified by nanoparticles and /or fire retardants
b) Relate and predict the real fire behaviour (e.g. in the Single Burning Item ,SBI) of polymeric materials using intrinsic properties measured in small scale apparatus such as the TGA (thermogravimetric analyzer), DSC (Differential Scanning Calorimeter) combined with EGA (evolved gas analysis such as FTIR) as well as in intermediate scale apparatus such as the cone calorimeter and tube furnace and
c) Explore the design of new fire safe materials.
These objectives expand beyond the current state of the art of fire retarded materials which is based on trial formulations that can only be evaluated doing large scale fire tests.

Overall self assessment

PREDFIRE made significant progress in a) quantitatively modelling the fire retarding action of nanoparticles regarding their shielding action on the surface of the pyrolysing nanocomposite polymer , b) modelling microscale measurements to mesoscale fire behaviour , c) modelling mesoscale to large scale behaviour and d) proposing promising combinations of nanoparticles , chemical (phosphinated based) fire retardant and intumescent paints. We were also invited by SPRINGER VERLAG to write a book on Nanocomposite polymers. We would like to suggest to the commission to fund the writing of this book as we have run out of time in this project given also the fact that there will be about 100,000 Euro surplus in the funding of the project owing to the variability of the exchange rate. Such an endeavour would enhance the dissemination.

1.2 Execution and major results of the PREDFIRE NANO project

The execution and methodologies of the project are reflected in the following diagram which also illustrates the interrelationships of the original research work packages 1 to 6. Work package 7 is the management work package and WP8 is an additional package (not shown in the diagram) representing a Russian partner associated with PREDFIRE through TTC funding.

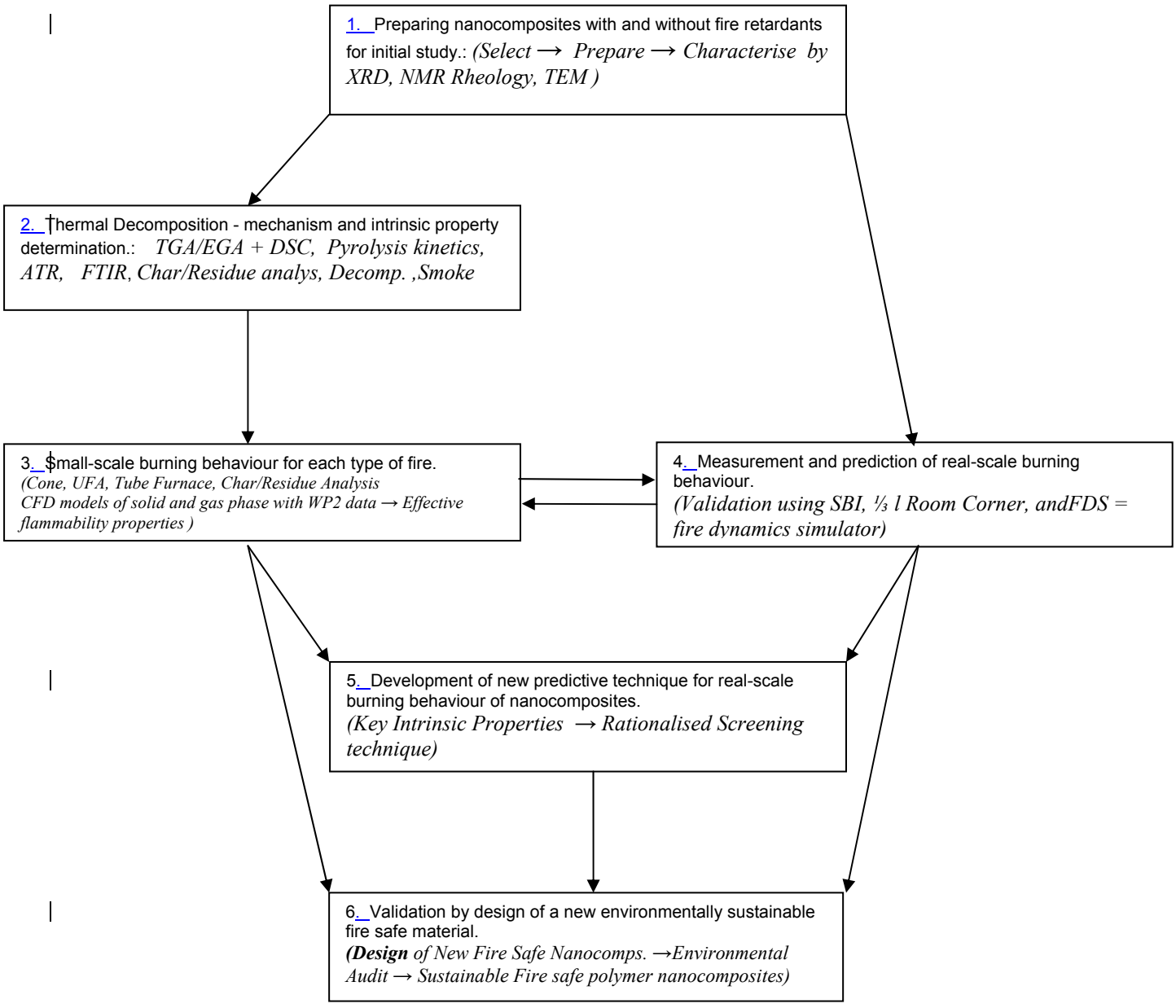

Figure 1 Presentation of work packages, measurements methodologies and interrelations between the work packages as having been executed in the PREDFIRE project

Summary of the work performed

The work performed followed mostly exactly the description of work packages (see Fig.1) as the deliverables testify. A brief summary of the work for each package follows :

- **WP1 (nanocomposite polymer formulation). List of all materials is included in the P2 periodic activity report :** In addition to more than forty (40) materials (exceeding the project plans) produced initially in WP1 another set of 50 samples was produced as required for the ignition apparatus in Un. of Edinburgh and the UFA in FireSERT. These materials include polymer based nanocomposite, fiber reinforced nanocomposites and intumescent coatings. Their nano monodispersion in WP1 has been obtained through XRD, NMR and Rheology and TEM. A correlation of these measurements has been obtained and published. During the third period, the ordering of large scale PP samples (for WP4) has been completed, and the large scale samples of flaxboard plus Char 17 have been delivered (for WP4). The main activity in the fourth period was the ordering and delivery of large scale PP samples (for WP4, large scale testing), and the completion of the delivery of the large scales of flaxboard plus Char 17 (for WP4, large scale testing).

- **WP2: (intrinsic properties). List of all measurements are included in the P2 periodic activity report.** In the fourth year, several measurements of specific heat and heat pyrolysis were performed using a horizontally oriented TGA/ DSC that is connected to FTIR. Moreover ATR measurements (using the FTIR apparatus) for the solid residue are conducted to characterise its composition. The Deliverable D2.2 demonstrated that only the rheological properties can be correlated with the degree of nanodispersion as measured in WP1. Following completion of the current measurements of heat of pyrolysis, ATR and FTIR, a list with flammability properties has been tabulated.

- **WP3**: **(intermediate scale experiments).** Deliverable D3.3 on methodologies for using intrinsic properties has been completed. Wood samples (Flax-board) plus char 17 and Sepiolite which were used for large-scale tests have been tested in the cone calorimeter. A numerical model was developed for studying the burning behaviours of wood and wood with char 17 and Sepiolite (D3.5). The toxicity measurements in the tube furnace have also been completed (D3.4)

- **WP4: (large scale experiments).** The large scale experiments in the SBI apparatus and I/3 scale ISO room have been completed (D4.1 and D4.2). The heat fluxes in the SBI experiment with inert have been reported. The FDS code has been used to predict these results and a final report with FDS's limitations is in D4.3.

- **WP5: (validation of predictive techniques).** Relationships between thermal decomposition and burning behaviour have been developed in WP3 and WP4. The heat transfer of the material, and particularly of nanocomposites, has been shown to be affected by the melt viscosity. The measurement of the intrinsic properties has been refined and robust protocols have been developed for consistency. Progress has been demonstrated rationalising the predictive techniques and demonstrating their capabilities.

- **WP6**: **(application for new materials).** Based on results from WP3, two formulations have been tested as a base for the development of new fire safe nanocomposites: PP+FR+NC and PA6+FR+NC. The development was driven by the modifications obtained on the intrinsic properties identified in WP5, namely the melt viscosity and the char strength. On these two selected formulations, the effect of polymer molecular weight and clay content were tested. (D6.2, D6.3, D6.4).

- **WP8 (millimetre wave spectroscopy for nanodispersion and temperature**). All tasks were accomplished except in deliverable D8.6 for the experiments in the cone calorimeter because the partner could not buy the required equipment without the funding available in advance. A nondestructive method is developed for determining the uniformity of nanoparticle distribution in plane parallel polymer samples. The method is based on the measurement of the capacitance of various areas of a sample. A maximal spatial resolution 1- 2 mm at frequencies of 10-100 kHz is achieved in these measurements. This method can serve as a basis for the design of a commercial device for the nondestructive control of the uniformity of nanoparticle distribution in plane parallel samples of polymers and ceramics. It is also shown that the measurement of reflection of millimeter-wave-band electromagnetic waves from plane parallel samples of nanopolymers allows for (a) remote determination of the uniformity of nanoparticle distribution in polymer samples (both low-loss and high-loss polymers). The degree of uniformity is determined over a surface area on the order of the wavelength of incident radiation (i.e., about a few millimeters). (b) remote determination of the surface temperature of the samples mentioned in item (a), including measurements through the flame. To this end, one uses the temperature dependence of the reflection coefficient of a sample.

1.3 Major results and impact on industry

The major achievements and results are summarized as follows:

1. **An impressive wealth of data** has been collected for six different fire retarded polymers PA6 , PP, PBT , EVA , Flaxboard + intumescent Char17, and PP +Flax fiber . The data include measurements for the characterization for monodispersity (XRD, TEM, NMR. Rheometry) , data for intrinsic flammability properties (TGA, DSC, MDSC, ATR, Char strength, Smoke point) , data in intermediate scale pyrolysis and flame (tube furnace , cone calorimeters) and large scale fire data (SBI test , 1/3 scale ISO room tests with different openings). All these data included in an edited CD provided to the commission are recommended that they should be published in a book.

2. **It was demonstrated that the monodispesrsity** of the nanocomposites can be characterised well by increased dynamic viscosity via Rheometry which gives consistent reulsts with the other techniques i.e. XRD, TEM, NMR. The Russian TTC partner also demonstrated that nonodispersity and uniformity can be measured using millimetre wavelength determination of eth dielectric properties of the nanocomposite polymer.

3. **Microscale to Mesoscale modelling** for nanocomposite polymers in fire: An important achievement was the development and demonstration of a methodology to relate microscale (intrinsic) properties to mesoscale (cone calorimeter) pyrolysis and burning. This is included with conclusions in Appendix A. A list of (mesoscale type) flammability properties for most of the materials in the present programme is provided in Appendix B.

4. **Mesoscale to Large scale modelling**: a methodology was developed to model the large scale behaviour from mesoscale and microscale properties using CFD (the Fire Dynamic Simulator FDS as proposed) modelling (see Deliverables 4.3.1 , 4.3.2) . However, it has not been completely successful because the FDS code has deficiencies not previously known. Namely, it predicts lower flame temperatures and soot and hence lower heat fluxes to the pyrolysing material which do not allow the fire to spread as the experiments show. For

this purpose we used an integral model developed in FireSERT and similarity parameters that can relate the mesoscale results to the large scale results.
Basically the FIGRA and SMOGRA in the SBI experiments are monotonic functions of two quantities (see M. Delichatsios "Upward Flame spread for correlating Standard SBI and ISO room tests "THERMAL SCIENCE ,11, PG.7-22, 2007, prepared as part of this work) :

A characteristic fire spread velocity $$U_s = \frac{L_m}{t_{ign}} \approx \frac{\dot{q}''^2}{t_{ign}} = \frac{PHRR^2}{t_{ign}}$$

And the smoke yield in the cone calorimeter: Y_s

Here $\dot{q}''$ is the Peak Heat Release Rate per Unit Area in the cone calorimeter at a selected imposed heat flux (e.g. 50 kW/m^2) , t_{ign} is the ignition time in the cone calorimeter at the same selected heat flux (e.g. 50 kW/m^2) . It is desirable to have lower values of $U_s = \frac{\dot{q}''^2}{t_{ign}}$ (being like FIGRA) and lower values of smoke yield Y_s (being like SMOGRA/ FIGRA). The values for all the materials are shown in Fig.1 .

Values of the ordinate, i..e the fire spread parameter $PHHR^2 / t_{ign}$ less than about 2000 ($kW^2 / m^4 s$) and of the abscissa less than 0.05 would be desirable and acceptable in practice as comparisons with ISO room and SBI tests have shown. ("Upward Flame spread for correlating Standard SBI and ISO room tests "THERMAL SCIENCE ,11, PG.7-22, 2007, prepared as part of this work). In that respect, we can make the following observations :

.

- The flaxboard +Char 17 (intumescent paint) and the EVA formulations with solid oxide and nanoparticles are the best performing materials. This observation explains why EVA+MH (orATH)+nanofiller is the only nanocomposite produced commercially.
- The Fire Retardant chemical OP1311 which induces intumescence inside the polymer is quite effective in lowering the fire spread parameter (ordinate in Fig. 1) but it increases or does not reduce the smoke yield.
- The nanofiller In PA6 is quite efficient in reducing the fire spread parameter (but not enough) and the smoke yield .
- Both nanofillers and the Fire retardants OP1311 do not increase the ignition time (not shown in Fig.1 directly) whereas the intumescent paint Char 17 does increase it considerably.

We may conclude from Fig.1 that the use of a combination nanofillers + Phosphinates (OP1311) + Char17 (intumescent layer) would provide the optimum fire retardant solution both for large scale fires as well as for the small questionable flammability tests UL94 and LOI index (as we expect and will be examining in other work).

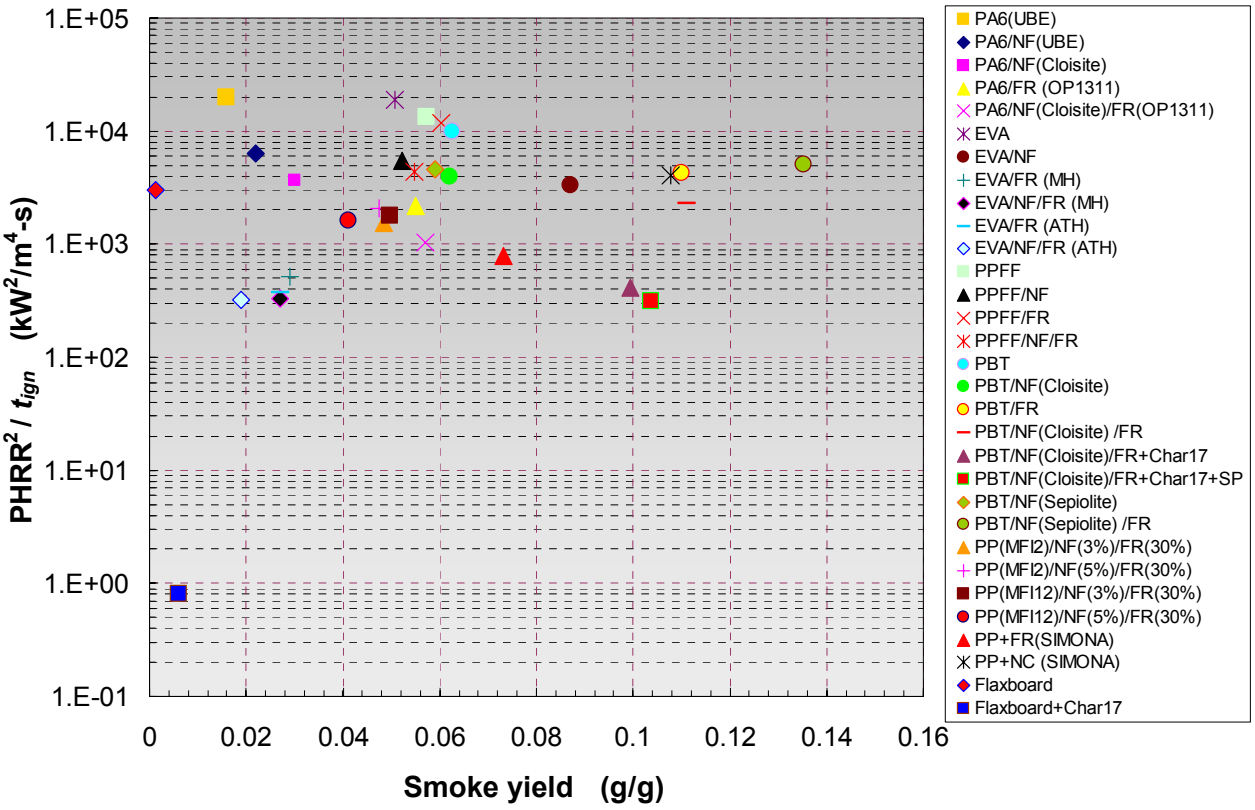

Figure 1. Characterisation of large scale fire behaviour of all materials tested in this program using two parameters for fire growth and smoke production deduced from data in mesoscale (i.e. cone calorimeter) experiments **.**

5. **Formulations of fire retardant plus nanocomposite: C**ombinations of Fire Retardant chemical and nanocomposite (e.g. PA6+OP1311+ Nano) have been shown to provide a product that reduces flammability (fire growth) , tendency to dripping and allows processability from raw or recyclable materials (as shown in WP6) . Two areas that have not completely been resolved in this work are related to the ease of ignition and smoke production. The only polymer formulation that is superb is EVA+MH(orATH) +nanofiller . However to make other nanocomposite polymer (NCP) formulations suitable substitutes for brominated fire retardants, ignition must be delayed. The phosphinate Fire Retardant (e.g.Exolit used here) causes earlier ignition than the NCP and produces twice as much smoke per unit mass pyrolyzed. One approach resulting from this programme is to apply on the surface of NCP a intumescent coating such Char 17 which has been provided by a partner in this programme. The following Figure shows that such an application increases the ignition time from 30s (for PBT+FR+Cloisite) to 100 s (for PBT+FR+ Cloisite +{Char 17}) and to 128 s (for PBT+FR+ Cloisite +{Char 17+2% sepiolite)}) sepiolite . Other important considerations such as durability of this surface application should be considered separately.

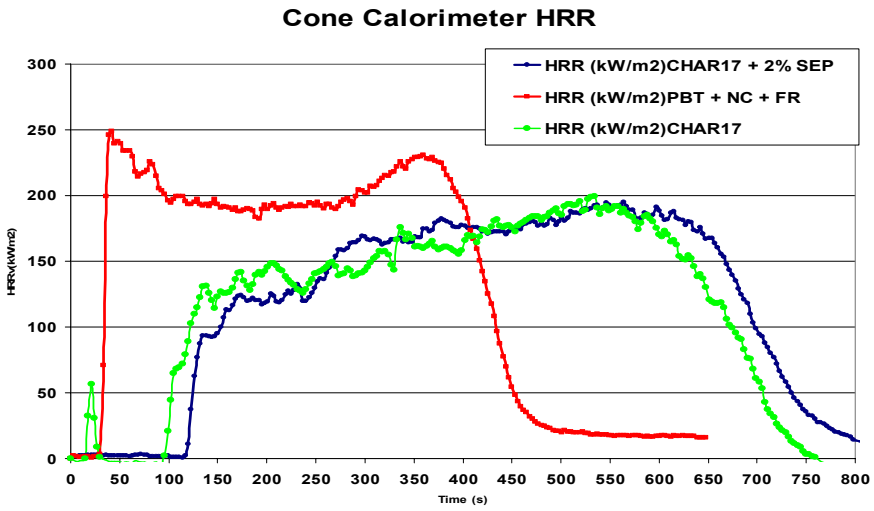

Figure 2. Heat release rates per unit area for a) PBT+FR+Cloisite: igniton time at 30 s b) PBT+FR+ Cloisite +{Char 17}: ignition time 100 s and c) PBT+FR+ Cloisite +{Char 17+2% sepiolite)}; ignition time 127 s . The sharp increase heat release rate coincides with the ignition time .

1.4 Recommendations

PREFIRE made a giant step in quantitatively characterising the action of nanoparticles and ist interaction with several phospinated fire Retardants (namely: aluminium diethylphosphinate (AlPi) , zinc diethylphosphinate (ZnPi) , melamine polyphosphate (MPP) , melamine cyanurate (MC) 0 as well as an intumescent paint. However two areas need further focusing:

- The fundamental parameters and chemistry for ignition and smoke (including toxic products) generation have to be addressed in more fundamental way from first principles
- The methodology to related microscale with mesoscale (Appendix A) has to be completed. A book exposing the present work to the industry and scientific community is desirable.

It is recommended to complete the development of a validated methodology for a material flammability certificate and develop molecular based modelling for the fire properties of polymers fire retarded by a combination of nanoparticles and metal phosphates or phosphinates . This achievement will fulfil the ultimate objective of fire research and the development of fire safe materials based on first principles, an aim far beyond the current state of the art.
The development of new materials and new fire retardants to replace, for example, brominated fire retardants makes imperative to develop new methods to characterize their flammability performance in mg quantities and also design fire safe materials based on first principles. We propose to effect this assessment by developing a methodology that can lead to a material flammability certificate. Such a certificate will allow the prediction of the fire behaviour of materials in real fires including fire growth and toxic (smoke and gases) production.
The molecularly based modelling techniques will include molecular dynamics and quantum chemistry. These are new areas showing great promise as the work demonstrates with Prof. Dlugogorski at the University of Newcastle Australia who specializes in fire chemistry (e.g. see his publication on "Quantum chemical Investigation of Formation of Polychlorodibenzo-p-Dioxins and Dibenzofurans from Oxidation and Pyrolysis of 2-Chlorophenol", J.Phys.Chem.A 2007,111,2653-2573). This is an outcome of recent grant related to molecular based modellingof organic pollutants: "(2006-2009) Discovery Project(Australia): Formation of organic pollutants in fires of treated and contaminated wood", **Dlugogorski**, Kennedy, Mackie and

Delichatsios (AU$600,000).). In such an investigation with Quantum Chemistry, B3LYP incorporated in the Gaussian 03 code will provide optimized geometries and harmonic vibrational frequencies of all transitions, all reactants and products . Moreover for the Molecular Dynamics, the computer program MD-REACT can be modified to solve the equations of motion for the molecules and nanoparticles (Nyden, M.R. and J.W.Gilman, Comp.and Theor. Polym.Sci.7:191-198, 1997).

4. CONSORTIUM MANAGEMENT and DISSEMINATION AND USE

ACTIVITIES AND RESULTS FOR WP7: Project Management, dissemination and exploitation

The first objective of this work package is to coordinate and manage the project and the day-to-day progress of the project using spreadsheets and relational databases. Namely, it will provide a communication medium between the project partners and the Executive Board. The Workpackage will consolidate project planning, work control, progress reports, milestone reports, cost statements and budgetary overviews using input from the Workpackage Leaders. This work package will also monitor and motivate the exploitation of the project results.

The second objective of this WP is to optimise the exploitation of the project results through the use of experimental and computational methodologies developed in other Work packages. Intermediate objectives are to obtain a thorough knowledge of the market conditions for the project products, to raise awareness of the problems which the project addresses, and to position the project as the solution of choice for those problems.

The last objective of this WP is to promote the dissemination of the project results in the European industrial and universal scientific communities

Deliverables

D7.1 Progress Report – Month 12
D7.2 Progress Report – Month 24
D7.3 Final Report – Month 44
D7.4 Exploitation & Dissemination Report - Month 24
D7.5 Exploitation & Dissemination Report - Month 44
D7.6 Draft of Technical Implementation Plan –Months 12
D7.6 Draft of Technical Implementation Plan –Month 24
D7.7 Preparation of Project Presentation and setting up of Project web site (internal and external pages)
D7.8 Final Plan for using and disseminating knowledge
D7.9 Report on raising public participation and awareness

Three meetings of the consortium including the Russian partner were held in 2008 In Lille (January 2008) in UCLAN (March 2008) and a final meeting in Ulster (December 2008) . The partners participated as invited speakers in several international conference to disseminate the results :

1. Fire retardant conference (19th Annual) BCC in Stamford Connecticut USA June 9-11 2008
2. Thirty -second International Combustion Institute Meeting , August 3-8 , Montreal Canada
3. 9th International Symposium on Fire Safety Science (IAFSS) , 21-26 September, Karlsruhe , Germany
4. International Modest –Workshop in China , Beijing: “Nano-filled Fire Retarrdant Polymers and Polymeric Composites” October 16-17 2008 , two invited talks.
5. 2008 Internatioanl Seminar on the Frontier Of Fire Safety Science , October 14-15 , 2008 , USTC , State Key Laboratory for Fire Science (SKLFS).

We are also palnning to presnt papers from PREDFIRE , the 20th Fire retardant conference (19th Annual) BCC in Stamford Connecticut USA a.and d FRPM 09 in Poland .

We were also invited by SPRINGER VERLAG to write a book on Nanocomposite polymers. We would like to suggest to the commission to fund the writing of this book as we have run of time in this project given also the fact that there will be about 100,000 Euro surplus in the funding of the project owing to the variability of the exchange rate. Such an endeavour would enhance D7.9.

PLAN FOR USING AND DISSEMINATION THE KNOWLEDGE.

Section 1 - Exploitable knowledge and its Use

We anticipate that a combination of intumescent phosphorous compound as Fire Retardant chemical together with nano filler and an intumesacent paint 9 E.g. Char 17) can be proposed for exploitation. We have had inquiries form CIBA about the project and some of us will participate in a new European project ENFIRO to investigate the possible replacement of Brominated Fire Retardants with environmentally (phosphinate +Nano+Intumescent) compatible ones.

Section 2 – Dissemination of knowledge

The dissemination activities section should include past and future activities and will normally be in the form of a table maintained by the coordinator or any other person charged with controlling the dissemination activities**.**

Overview table

Planned/ actual Dates	**Type**	**Type of audience**	**Countries addressed**	**Size of audience**	**Partner responsible /involved**
16/9/06	*Conference Modest*	*Research , Industry*	*International*	*Hundred*	*All*
28/3/07	*Joint meeting with NANOFIRE*	*Research Industry*	*International*	*Hundred*	*All*
3/7/2007	*PREDFIRE NANO Seminar*	*Research Industry*	*International*	*Hundred*	*All*
9-11 2008	Fire retardant conference (19th Annual) BCC in Stamford Connecticut USA June	*Research and Industry*	*International*	*Hunderd*	*Ulster, ENSCL ,UCLA N, Iris Verici*
August 3-8	Thirty -second International Combustion Institute Meeting ,Montreal Canada	*Research and Industry*	*International*	*Thousand*	*All*
September 21-26	9th International Symposium on Fire Safety Science (IAFSS) Karlsruhe , Germany	*Research and Industry*	*International*	*Four Hundred*	*Al*
October 16-17 2008	International Modest – Workshop in	*Research and Industry*	*International*	*Two Hundred*	

Planned/ actual Dates	Type	Type of audience	Countries addressed	Size of audience	Partner responsible /involved
October 14-15 , 2008	China , Beijing: "Nano-filled Fire Retarrdant Polymers and Polymeric Composites", two invited talks. 2008 Internatioanl Seminar on the Frontier Of Fire Safety Science , USTC , State Key Laboratory for Fire Science (SKLFS).	*Research and Industry* *Research and Industry*	*International* *International*	*Two Hundred* *One hundred*	*Ulster, Uclan, ENSCL* *all*
10/12/06 *2007*	*Publications* *See list on next page*	*Research / Industry*			*All*
Available	*Project web-site* www.engj.ulst.ac.uk/predfire/ Fire Safety Journal Fire and Materials etc, More than thirty publications presented	*Public / research industry*	*International*		*All*
24/09/06	*Congress JEPO*	*Research*	*International*		*ENSCL*

LIST OF PUBLICATIONS

1. J. Zhang, J. Hereid, M. Hagen, D. Bakirtzis, M.A. Delichatsios, A. Fina, A. Castrovinci, G. Camino, F. Samyn and S. Bourbigot, Effects of Nanoclay and fire retardants on fire retardancy of a polymer blend of EVA and LDPE, *Fire Safety Journal, Under Review, 2007.*

2. T. Beji, J. Zhang, and M. Delichatsios, Determination of soot formation rate from laminar smoke point measurements, 5th Mediterranean Combustion Symposium, Monastir, Tunisia, September 9-13 2007 *(*accepted for publication in *Combustion Science and Technology, 2008).*

3. M. A. Delichatsios and J Zhang, Pyrolysis of a finite thickness composite material, in Press, *International Journal of Heat and Mass Transfer, 2008*.

4. Delichatsios M.A., Zhang J., Hereid J., Hagen M., Bakirtzis D.Flammability Assessment of Fire Retarded Nordic Spruce Wood using Thermogravimetric Analyses and Cone Calorimetry, *paper submitted to Fire and Materials, 2007*

5. D. Bakirtzis , M.A. Delichatsios…Nanoclay effect on flammability properties of poly(1,4-butylene Terephthalate) mixed with phosphorus based flame retardant paper submitted to *Polymer Interflamm 2007, Fire and Materials ,2008*

6. D. Bakirtzis , M.A. Delichatsios Fire retardant properties of sodium bicarbonate (NaHCO3) on Mediterranean forest species paper submitted to *Acta Chimica 2008*

7. A A Stec and T R Hull, Assessment of fire toxicity from polymer nanocomposites. *Fire Retardancy of Polymers: New Strategies & Mechanisms, Royal Society of Chemistry* (in Press Mar 08)

8. A A Stec and T R Hull, Toxic Combustion products from fire retarded nanocomposite polymers. Submitted for peer review to the *Proceedings of the 5th International Seminar on Fire and Explosion Hazards, Edinburgh, 2007*.

9. S Nazare, T R Hull, B Biswas, F Samyn, S Bourbigot, C Jama, A Castrovinci, A Fina and G Camino, Study of the Relationship Between Flammability and Melt Rheological Properties of Flame Retarded Poly (Butylene Terephthalate)s Containing Nanoclays. *Fire Retardancy of Polymers: New Strategies and Mechanisms, Royal Society of Chemistry* (in Press Mar 08).

10. S Bourbigot, S Duquesne, G Fontaine, S Bellayer, T Turf and F Samyn. Characterization and reaction to fire of polymer nanocomposites with and without conventional flame retardant. *Molecular Crystals & Liquid Crystals*, in press 2008.

11. F Samyn, S Bourbigot, C Jama, S Bellayer. Flame retardancy of polymer clay nanocomposite: Is there an influence of the nanomorphology? *Polymer Degradation and Stability,* in press 2008.

12. F Samyn, S Bourbigot, C Jama, S Bellayer, S Nazare, R Hull, A Castrovinci, A Fina and G Camino. Crossed characterisation of polymer-layered silicate (PLS) nanocomposite morphology: TEM, X-ray, diffraction, Rheology and solid state nuclear magnetic resonance measurements. *European Polymer Journal,* under review 2008.

13. M. Delichatsios, M. Hagen, J. Zhang, D. Bakirtzis, and A. Ramani, Thermo gravimetric Fourier transform-infra red (TGA-FTIR) investigation of polyamide 6 (PA6) nanocomposites, *Fire Retardants 2008 conference*, London, 2008

14. J. Beji, J Zhang, and M. A. Delichatsios, Development of a Soot Formation and Oxidation Model in Laminar Nonpremixed Flames, *9th IAFS*S, Under Review, 2008

15. J. Zhang, M.A. Delichatsios, J. Hereid, M. Hagen, D. Bakirtzis and S. Bourbigot, Numerical studies of pyrolysis of a polyamide 6 nanocomposite, *32nd International Symposium on Combustion*, Under Review, 2007

16. J. Zhang, M. A. Delichatsios, J. Hereid, M. Hagen and D Bakirtzis, Heat impact and flame heights from fires generated in single burning item tests, *Interflam 2007*, 2007, pp. 441-452.

17. D. Bakirtzis, A. Schmitt, M. McKee, J. Zhang, M. A. Delichatsios, Nanoclay effect on flammability properties of poly (1,4 -butylene terephthalate) mixed with phosphorus based fire retardant, *Interflam 2007*, 2007, pp. 79-88.

18. J. Zhang, J. Hereid, M. Hagen, D. Bakirtzis, M.A. Delichatsios, A. Castrovinci, A. Fina, G. Camino, R. Carvel, J. Torero, R. Hull, S. Nazare, A. Stec, B. Biswas, S. Bourbigot, F. Samyn and C. Jama, Experimental and numerical studies of pyrolysis of polyamide nylon nanocomposites, presented at the *11th European Meeting on Fire Retardant Polymers, 2007.*

19. J. Zhang, J. Hereid, M. Hagen, D. Bakirtzis, M.A. Delichatsios, A. Castrovinci, A. Fina, G. Camino, R. Carvel, J. Torero, R. Hull, S. Nazare, A. Stec, B. Biswas, S. Bourbigot, F. Samyn and C. Jama, Effect of nanofillers and fire retardant on the fire retardancy of EVA, poster at the *11th European Meeting on Fire Retardant Polymers, 2007.*

20. J. Zhang, M. A. Delichatsios, J. Hereid, M. Hagen, M., Bakirtzis and A. G. Venetsanos, Numerical studies of dispersion and flammable volume of hydrogen in enclosures, *2nd International Conference on Hydrogen Safety, 2007.*

21. J. Zhang, M. A. Delichatsios, J. Hereid, M. Hagen, and D. Bakirtzis, Determination of the convective heat transfer coefficient, *5th International Seminar on Fire and Explosion Hazards, 2007.*

22. F. Samyn, S. Bourbigot, C. Jama, S. Nazare, R. Hull, A. Castrovinci, G. Camino, M. Hagen, M. A. Delichatsios. Development et characterisation de nanocomposite PA6/Argile en vue de l'amelioration des proprietes feud u PA6. *«34èmes Journées d'Etudes des Polymères, JEPO 34 »,* Université de Bretagne Sud, Lorient (France), Septembre 2006.

23. F. Samyn, S. Bourbigot, C. Jama, S. Nazaré, R. Hull, A. Castrovinci, G. Camino, M. Hagen and M. A. Delichatsios. Development et characterisation de nanocomposite PA6/Argile en vue de l'amelioration des proprietes feud u PA6. *«34èmes Journées d'Etudes des Polymères, JEPO 34 »,* Université de Bretagne Sud, Lorient (France), Septembre 2006.

24. S. Nazare, T. R. Hull, B. Biswas, S. Bourbigot, A. Castrovinci, A Fina, G. Camino. Study of relationship between rheological and flammability properties of flame retarded poly (butylene terephtalate) containing nanoclays. *18th BCC Conference – Recent Advances in Flame Retardancy of Polymeric Materials*, Vol 18, Stamford, CT (Etats-Unis, Mai 2007.

25. J. Zhang, J. Hereid, M. Hagen, D. Bakirtzis, M. A. Delichatsios, A. Castrovinci, A. Fina, G. Camino, T. R. Hull, S. Nazare, A. A. Stec, B. Biswas, F. Samyn, S. Bourbigot and C Jama. Numerical and experimental studies of pyrolysis and polyamide nanocomposite. *11th European Conference on fire Retardancy and Fire Protection of Materials – FRPM'07*, University of Bolton, Bolton (Royaume-Uni, Juillet 2007.

26. S. Nazare, T.R. Hull, B. Biswas, F. Samyn, S. Bourbigot, C. Jama, A. Castrovinci, A. Fina and G. Camino. RHEOLOGICAL PROPERTIES AND ITS INFLUENCE ON FLAMMABILTY OF POLYBUTYLENETEREPHALATE COMPOSITES *«11th European Conference on Fire Retardancy and Fire Protection of Materials – FRPM'07 »,* University of Bolton, Bolton (Royaume-Uni), Juillet 2007

27. A. Fina, A. Castrovinci, G. Camino, F. Samyn, S. Bourbigot, C. Jama, M .Hagen, D. Bakirtzis, M.A. Delichatsios, S. Nazare, T.R. Hull, B. Biswas, R. Carvel, J. Torero. EFFECT OF NANOFILLERS AND FIRE RETARDANTS ON POLYPROPYLENE*«Workshop PredFire-Nano »,* University of Bolton, Bolton (Royaume-Uni), Juillet 2007

28. S. Nazare, T.R. Hull, B. Biswas, F. Samyn, S. Bourbigot, C. Jama, A. Castrovinci, A. Fina, G. Camino EFFECT OF NANOFILLERS AND FIRE RETARDANTS ON POLYBUTADIENETEREPHTALATE *«Workshop PredFire-Nano »,* University of Bolton, Bolton (Royaume-Uni), Juillet 2007

29. F. Samyn, S. Bourbigot, C. Jama, S. Bellayer, A. Fina, A. Castrovinci, G. Camino, M. Hagen, D. Bakirtzis, M.A. Delichatsios, S. Nazare, T.R. Hull, B. Biswas, R. Carvel, J. ToreroCOMBINATION FLAME RETARDANT-CLAY: SYNERGISTIC EFFECT? *«Workshop PredFire-Nano »,* University of Bolton, Bolton (Royaume-Uni), Juillet 2007

30. F. Samyn, S. Bourbigot et C. Jama Mechanism of protection of intumescent PA-6 nanocomposite *« 9th International Symposium on Polymers for Advanced Technologies »,* Shanghai (China), Octobre 2007

31. S. Bourbigot, G. Fontaine, S. Duquesne, F. Samyn, T. Turf et S. Bellayer Flame retardancy of polymer nanocomposite with and without flame retardants. *« 235th National American Chemical Society Meeting »,* 2 pages, Nouvelle Orléans, LA (Etats-Unis), Avril 2008.

32. Zhang, J., Delichatsios, M., and S. Bourbigot, Experimental and numerical study of the effects of nanoparticles on pyrolysis of a polyamide 6 (PA6) nanocomposite in the cone calorimeter, *Combustion and Flame*, Accepted for publication, 2009

33. Zhang, J., Delichatsios M,, Assessment of Fire Dynamics Simulator for Heat Flux and Flame Heights Predictions from Fires in SBI Tests, *Fire Technology*, Corrected proof, 2009

34. Zhang, J., Delichatsios, M., Determination of the convective heat transfer coefficient in three-dimensional inverse heat conduction problems, *Fire Safety Journal*, Corrected proof, 2009
35. Zhang, J., J. Hereid, M. Hagen, D. Bakirtzis, M.A. Delichatsios, A. Fina, A. Castrovinci, G. Camino, F. Samyn, S. Bourbigot, Effects of Nanoclay and fire retardants on fire retardancy of a polymer blend of EVA and LDPE, *Fire Safety Journal*, Corrected proof, 2008

36. Zhang, J., Dembele, S., Wen, J., Delichatsios, M., Application of a statistical narrow band model to CFD Modelling of Upward Flame Spread over PMMA walls, *Journal of Applied Fire Science*, 16:1-19, 2007.

Appendix A
Microscale to mesoscale testing and modelling

Micro to Mesoscale Testing and Modeling for Nanocomposite Polymers in Fires

By
Michael A. Delichatsios and Jianping Zhang
FireSERT , University of Ulster

Abstract

A challenge for fire safety is to reduce the fire hazards (i.e. heat fluxes and toxicity) by reducing the flammability of the source material through the design and modification of commonly used materials such as polymers to make them more fire resistant and less toxic than the base polymer materials. The modification of a polymer can be obtained by the addition of fire retardant chemicals and nanoparticles. Because it is difficult to make new nanocomposite polymers in large quantities, it is essential to determine the fire behaviour of new formulations (even hopefully in large scale) using microscale quantities (mg mass) and experimental methods such as TGA (Thermogravimetric Analyzer) , DSC (Differential Scanning Calorimeter), MDSC (Modulated DSC), FTIR (Fourier Transform Infrared Radiometry) , ATR (Attenuated Total Reflection) , and Rheometry that can provide information about the degradation of the solid phase and the composition of the gaseous products. Although these measurements have been available for a long time, it is only in the last decade (starting with a proposal to FAA) that a concerted effort is being made to quantitatively relate these microscale measurements with measurements in mesoscale apparatus (such as the tube furnace, cone, and Universal Flammability Apparatus (UFA)). This challenge, progress and needs for further work are summarized in this review with the further step of relating the mesoscale measurements to large scale fires (e.g. Single Burning Item test) left out. The present subject is focused on nanocomposite polymers, although some comparative data are included for nanocomposite polymers that are mixed with phosphorous-based intumescent fire retardants (e.g. exolit). Rheometry and TGA/ATR for the solid residue can be used to characterize melting and consistency of char. TGA/DSC/MDSC provide information about the thermal and transport properties and heats of melting and pyrolysis. TGA /FTIR (or mass spectroscopy (MS), not discussed in this review) provide the composition of the pyrolysis gases. These measurements are consistent and can be used for the quantitative prediction of behaviour in the mesoscale experiments (Tube Furnace, Cone, UFA). However, the tendency of nanoparticle additives to form a layer as soon as pyrolysis starts (in mesoscale or large scale experiments) requires a new method and model to characterise the reduction of mass loss rates caused by the shielding effects of the layer.

Table of Contents

1. Introduction

This article presents a review of the progress relating flammability measurements and properties deduced from microscale experiments of mg size samples with measurements obtained from

mesoscale experiments of sample size about 100 g. We present a comprehensive and integrated approach based on sound scientific method yet practical for assessing the flammability of nanocomposite polymers in the early stage of their formulations where only mg order quantities are available. Our approach does not extend to quantum chemistry of molecular dynamics to determine flammability properties *ab initio* because their use is still not feasible even in simplified situations. We also do not include in this article how the properties determined from microscale and mesoscale experiments can be used to determine the fire behaviour in large real fires, where the turbulent buoyancy flow can change the flammability impact for different materials concerning the generation of heat fluxes and production of toxicity gases such as CO and HCN; these studies will be included in other reports and papers.

The development of new materials and new fire retardants to replace brominated fire retardants makes it imperative to develop new methods to characterize their flammability performance in mg quantities and also to design fire-safe materials ab initio. We envision to effect this assessment by developing a methodology that can lead to a material flammability certificate. Such a certificate will allow the prediction of the fire behaviour of materials in real fires including fire growth and toxic (smoke and gases) production. This methodology is emerging from long experience in material flammability and fire dynamics by the authors and others and is supported by recent work in the European PREDFIRE NANO, FIRENET project and EPSRC (UK) and other industrial grants. The contribution of participants in these projects is greatly appreciated.

A proposed list of measurements follows together with the appropriate measuring equipment:

Microscale experiments:

- Tendency to dripping (based on rheology)
- Solid degradation in mg scale (using TG,DSC and MDSC) for heat of pyrolysis and specific heat)
- Solid residue analysis at different temperatures using TG /ATR
- Gaseous products in mg scale (using TGA/FTIR/MS for toxicity and ignition kinetics)

Mesoscale experiments:

- Tube Furnace (toxicity)
- Cone calorimeter in standard atmosphere (to assess the effectiveness of nano particles and intumescent Fire Retardants and also measure heat release rates and product yields)
- Special calorimeter (Universal Flammability Apparatus to assess combustion in under-ventilated conditions and evaluate tendency for dripping and char strength by performing experiments in vertical orientation)

It is intended to use these properties for the assessment of alternative FRs (including nanoparticles, phosphates and inorganic metal oxides) in comparison with brominated fire retardants by quantitatively assessing:

- Tendency to dripping
- Low heat release rate
- Late ignition
- Strength of char (e.g. to avoid erosion)
- Low smoke including the smoke point of the material
- Low toxicity and possibly, corrosivity

Finally, based on these properties the global effect of these materials in fire can be addressed by quantifying:

- Their behaviour in standard tests (UL94 , LOI, SBI)
- Their behavior in large fires
- Impact on life and property safety and damage.
- Recyclability

These tasks are not included in this review.

A brief outline of the structure of the paper is:

Section 2: Description of materials (for a specific investigation that is used to demonstrate the procedure)

Section 3: The microscale properties and associated instruments are presented first:

1. Rheometry (dynamic viscosity)
2. TGA in air and in nitrogen (pyrolysis kinetics in air and nitrogen)
3. DSC and MDSC (heat of pyrolysis and specific heat until pyrolysis occurs)
4. TGS/ FTIR or MS (toxicity, ignition chemistry, heat of combustion)
5. ATR (composition of residue at different temperatures)

Section 4: The mesoscale properties and measurements follow:

1. Tube furnace (toxicity)
2. Regular cone (thermal properties and physical behaviour , products of combustion in normal air, effective heat of combustion)
3. UFA): same as cone but in addition burning in different oxidizer atmospheres.

Section 5: Prediction of mesoscale behaviour using microscale measurements,

1. flammability properties
2. numerical modelling
3. validation using various nanocomposite polymers

2. Materials

The materials included in this review for illustration are nanocomposite polymers combined with intumescent commercial phosphorous fire retardants. In this article different base polymers (e.g. PA6, PBT, PP and EVA) will be mentioned for illustrating the methodology but the focus will be on PA6. For the present purpose, the composition of a PA6 nanocomposite is described next to make the development of the presnt methodology more clear.

Polyamide 6 (PA6, by Rhodia) was modified with a nanoclay (Cloisite 30B by Southern Clay) and a flame retardant chemical (OP1311 by Clariant). In total, combinations of the polymer (PA6), nanoclay (NC), and fire retardant (FR) provide 4 formulations, i.e., PA6, PA6/NC, PA6/FR, PA6/NC/FR. In addition, commercially available PA6 nanocomposite with 2.5 wt. % clay by UBE was also used as a reference material. Compounds of all the materials were prepared at Centro di Cultura per l'Ingegneria delle Materie Plastiche (CDCMP) in Italy by melt blending in a Leistritz

ZSE 27 co-rotating intermeshing twin screw (27 mm) extruder with length/diameter ratio of 40. The Screw speed was set to 200 rpm, the mass flux at 10 kg/h and the processing temperature range from 210 to 230 ^{o}C. The polymer blend was loaded in the main feed and the fillers were added to the molten polymer by means of a gravimetric side feeder. The extruded materials were cooled in water and then pelletised. The compositions of all formulations are shown in Table 1.

Table 1. Compositions of all PA6 based formulations

Material	Abbreviation	NC (wt. %)	FR (wt. %)
PA6	PA6_R	-	-
PA6+OP1311	PA6+FR	-	18
PA6+Cloisite 30B	PA6+NC	5	-
PA6+OP1311+Cloisite 30B	PA6+FR+NC	5	18
PA6+Clay (UBE)	PA6+NC(UBE)	2.5	-

The dispersion morphology of prepared materials was studied with a multitechnique approach, by means of Rheology, Scanning Electron Microscopy (SEM), X-Ray Diffraction (XRD), and Nuclear Magnetic Resonance (NMR). The results of these tests showed that the so formulated PA6 nanocomposites used in the present study are fully exfoliated [1-2].

3. Microscale experiments and measurements

3.1 Rheology – viscosity (affecting dripping and structure of the char layer)

The dynamic viscosity and storage modulus of the melt polymer can characterise a) the degree of dispersity (i.e. intercalation) of the nanocomposite polymer [1,2], b) the dripping tendency in mesoscale or large scale fires [3,4] and c) the structure of the char layer formed during pyrolysis in mesoscale or large scale fires [5-7].

Rheological measurements were carried out at a Dynamic Analyser Rheometer RDA II from Rheometrics. Parallel plate geometry with a plate diameter of 25 mm was used to perform the tests where thin films of materials of 1mm thickness were inserted. To ensure the viscoelastic region, linear rheological measurements were performed at a frequency range of 0.1–100 rad/s. Elastic complex viscosities (η^*) were obtained at 240 °C. The temperature control was accurate to within ±1 °C. Experiments were conducted under a nitrogen atmosphere in order to avoid oxidative degradation of the specimen.

A comparison of the complex viscosities for PA6, PA6+NC, PA6+FR, and PA6+NC+FR is shown in Figure 1. The steady state viscosity behaviour of PA6 shows perfect Newtonian behaviour whereas the absolute value of the melt viscosity of the PA6+NC sample is significantly higher than that of neat PA6, particularly at low shear rates, indicating that the nanostructure of the nanocomposite consists of a percolated network superstructure of exfoliated platelets [1,2]. The complex viscosity of the PA6+NC sample, however, decreases sharply with increasing frequency, exhibiting pronounced shear thinning with a shear thinning component η = - 0.42. This implies a higher extent of silicate exfoliation on the nanoscale with a macroscopic preferential orientation of clay layers [1, 2]. This was also verified by XRD (X-Ray Diffraction) analysis of PA6+NC, which shows complete disappearance of the clay peak, suggesting exfoliated nanodispersion within the polymer matrix.

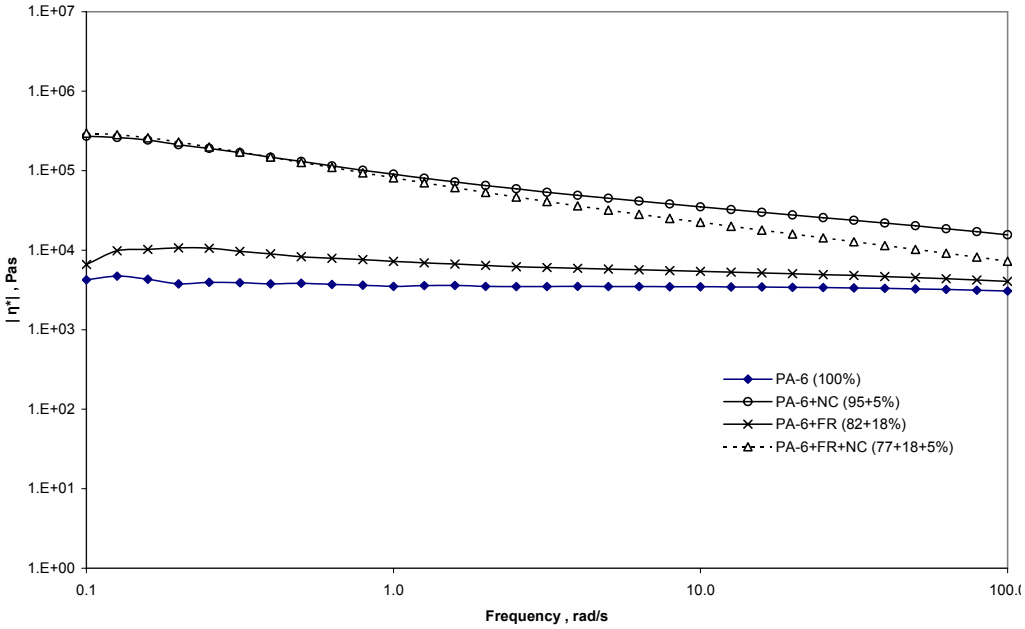

Figure 1. Complex viscosity curves for PA6, PA6+NC, PA6+FR, and PA6+NC+FR.

The structural network formed in nanocomposites (PA6+NC) is further emphasised by the behaviour of the storage modulus (G'), which is extremely sensitive to morphological state. The storage (G') and loss (G") moduli are plotted against frequency in Figure 2. Compared to PA6, the storage modulus of PA6+NC is increased by a factor of 200. This behaviour may be due to an elastic-dominant response of clay platelets on the rheological behaviour at low frequencies. At low frequencies, the storage modulus is higher than the loss modulus, suggesting more solid-like behaviour as compared to neat PA6. In contrast, at higher frequencies, the storage modulus is lower than the loss modulus indicating that the effect of clay particles on the rheological behaviour is weak and that the segmental motion of polymer molecular chains is dominant. The frequency at which G" crosses G' curve is called cross-over frequency and is characteristic of filler volume fraction. With addition of FR, the shear thinning component of PA6+NC is further increased to η=-0.56. As shown in Figure 2c, the storage modulus for PA6+NC+FR is slightly increased whereas the loss modulus is in fact reduced. This type of rheological behaviour may suggest that with increasing volume fraction the clay platelets or aggregates are more hindered in their rotation and movement, leading to a structure that can cause solid-like behaviour. It can also be seen that with the formation of more solid-like network structure, the cross-over frequency for PA6+NC+FR shifts towards a higher frequency 7.94 rad/s compared to 1.58 rad/s for PA6+NC.

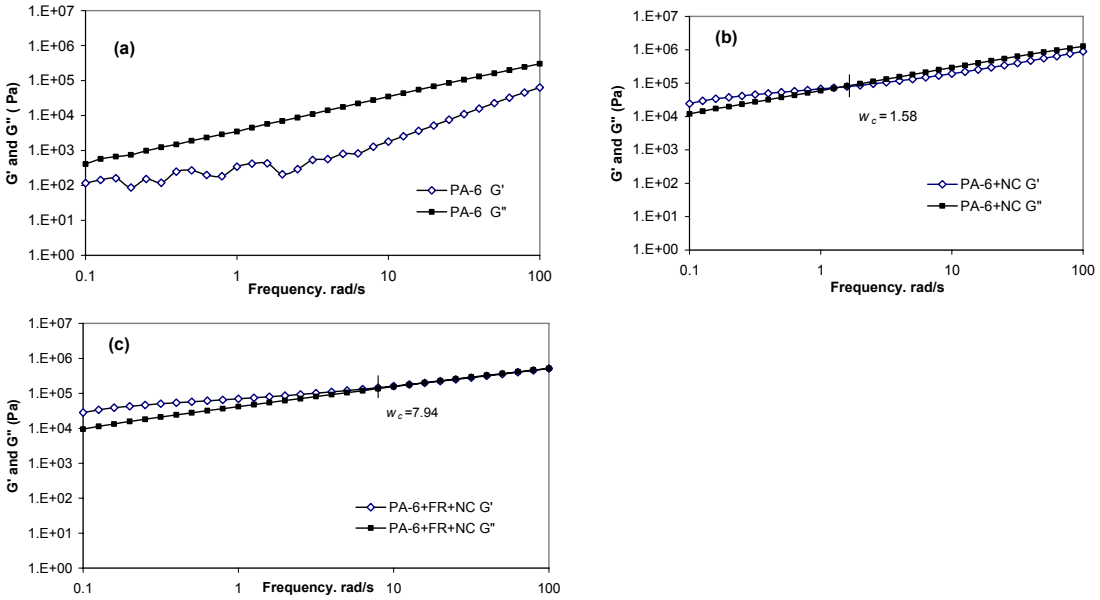

Figure 2. Storage modulus and loss modulus for PA6, PA6+NC, and PA6+NC+FR.

The melting behaviour can be extracted from the dynamic viscosity [3,4]. The dynamic viscosity also affects the morphology of the char, which may improve the shielding efficiency from the fire by the nanoparticle layer formed on the polymer [5-7].

3.2 TGA/ DSC and Modulated DSC

3.2.1 TGA/ DSC for heat of melting and heat of pyrolysis

Table 2 summarises properties measured by DSC (through heat flow measurements) for the materials in this illustration, including glass transition temperature, T_g, melting temperature, T_m, crystallisation temperature, T_{crys}, heat of melting, ΔH_m, and heat of crystallisation, ΔH_{crys}. The presence of clay in PA6+NC(Cloisite 30 B) seems to have an effect merely on the phase (γ or α) formed and the temperature of crystallization, whereas PA6+NC(UBE) does have a higher crystallisation temperature, heat of melting, and heat of crystallisation. Addition of FR seems to have no significant effects on these properties.

Table 2. Summary of properties measured by DSC at CDCMP for different materials

	T_g (^oC)	T_m (^oC)			T_{crys} (^oC)	ΔH_m (J/g)	ΔH_{crys} (J/g)
			γ	α			
PA6	54		214	220	186	68	65
PA6+NC	52	211	213	220	190	68	65
PA6+NC(UBE)	53	208	217	220	193	79	70
PA6+FR	54		214	219	186	63	62
PA6+NC+FR	52	210	212	219	186	70	62

The heat of pyrolysis was measured at the University of Ulster using a Mettler Toledo TGA/SDTA851^e measuring module, with temperature accuracy ±0.5 °C and temperature reproducibility of ±0.3°C. All the samples weighted to a Mettler Toledo XS205 Dual Range Analytical Balance were approximately 20.0±0.10 mg. The samples were placed in an alumina (Al_2O_3) pan (with no lid) of 70µl volume capacity and heated under a dynamic linear rate of 10

°C/min, in 50ml/min nitrogen (N_2) flow, from 25°C to 700°C. Measuring the heat of pyrolysis is challenging. The heats of pyrolysis obtained at Ulster are about half the value obtained in a recent paper which we consider more reliable [8].

3.2.2 Modulated DSC for specific heat, heat of melting

Modulated DSC by varying the furnace temperature sinusoidally has been used to determine the specific heat of PA6 materials. (similar measurements have been performed for Polypropylene nanocomposites). The materials were heated from -80 to 250 °C at 2 °C/min. The reversible signal recorded during the experiment is related to the specific heat of the sample. The specific heat values versus temperature for the different PA6 based formulations are given in Figure 3, showing no significant differences between different formulations. The peaks noted on the specific heat curves correspond to the transition from the solid to the liquid states.

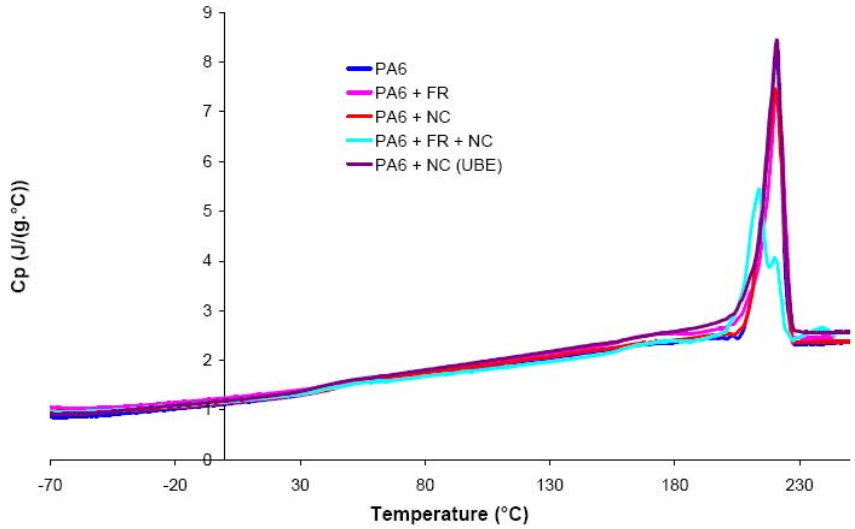

Figure 3. Measured specific heats of PA6 materials in the modulated DSC apparatus

The measured values of specific heat and heat of melting (as listed in Table 2) have been used to predict the heating and pyrolysis behaviour of 100mg samples of the materials in the cone calorimeter in section 6..

3.3 TGA/FTIR/ATR

Thermogravimetric analysis (TGA) experiments were carried out in Nitrogen and air to evaluate the degradation of the polymers as a function of temperature. The TGA Experiments were carried out in a Perkin Elmer Pyris 1 TGA apparatus, from 20-800 °C with a heating rate of 20 °C min^{-1} under a flow rate of 75 cm^3 min^{-1} of synthetic air or nitrogen. Each sample, in the form of powders weighing 10mg ± 0.01 mg was placed in a platinum pan, vertically mounted in the TGA. In addition to the TGA measurements, the gaseous products of the degradation were measured by connecting an FTIR (Fourier Transform Infrared Radiometer) apparatus to the TGA. Finally, the condensed phase drawn from the TGA at different temperatures was analysed by ATR (Attenuated Total Reflection) . These results are described next.

3.3.1 Degradation behaviours in N_2

Thermogravimetric analyses were first performed in nitrogen at different heating rates (1, 2, 5, 10 and 20 °C/min). Figure 4 shows a comparison of the weight loss and weight loss rate for different formulations for the heating rate of 10 °C/min. Note that similar results obtained for the other heating rates are not reported here fore the sake of brevity. The curves for PA6 and PA6+NC depict a one-stage degradation process. From the TGA curves, it seems that the inclusion of the nanoclay alone does not alter the thermal degradation behaviour of PA6 apart from its influence on increased char (residual mass) formation, as also observed by others [9,10]. The inclusion of FR chemical on the other hand (PA6+FR and PA6+FR+NC) changes the degradation behaviour by lowering the degradation temperature (increased degradation rate) in an additional step around 300-350 °C (15-20 min). This low temperature weight loss does not match the weight loss curve for OP1311 in Figure 5, which shows a single main degradation step with maximum weight loss rate at 460 °C. This fact evidences for an interaction between PA6 matrix and OP 1311, leading to the low temperature weight loss stage.

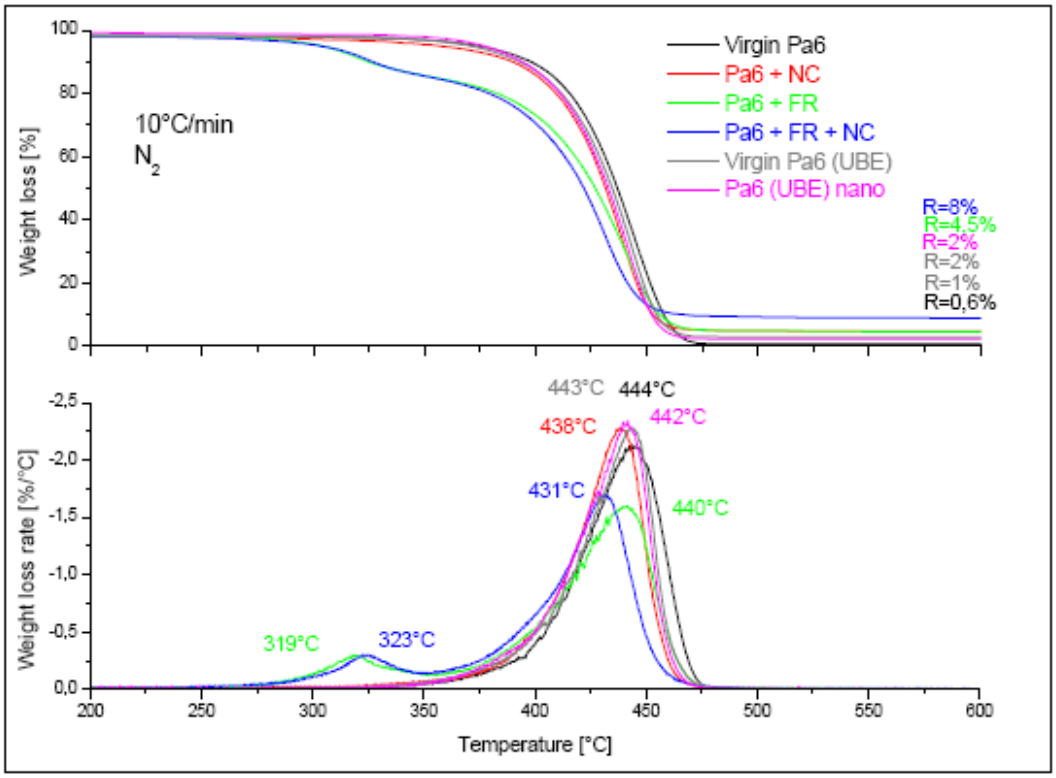

Figure 4. TG/DTG curves of PA6, PA6+NC, PA6+FR and PA6+FR+NC in nitrogen.

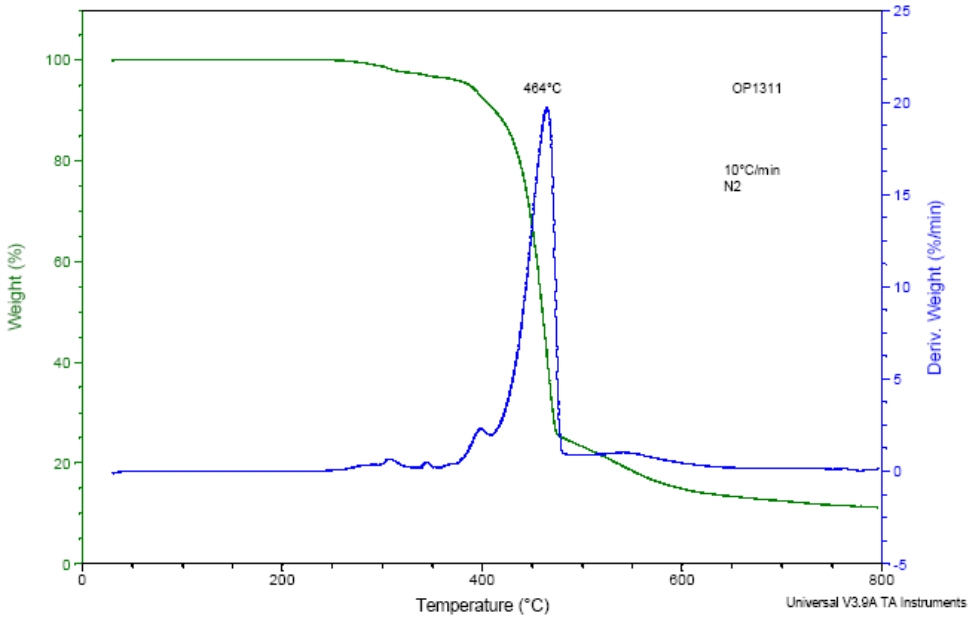

Figure 5. TG/DTG curves for OP1311 by Clariant.

It is likely that the presence of phosphorous and/or nitrogen in OP 1311 did catalyze the degradation of the PA6 polymer and thereby lowered the onset temperature. The mechanism is probably through electron capturing and transport by the more electropositive phosphorus and/ or nitrogen (from the FR), from the hydrocarbons of the polymer monomer (ε-caprolactam) or to the competitive electron sharing with the amide group of the monomer. These more electropositive elements also promoted to some extent the char formation through network cross-linking.

3.3.2 Degradation behaviours in Air

Figure 6 presents the TG/DTG curves of the PA6 materials in air, again for a heating rate of 10 ^{o}C/min. The thermal degradation of PA6 occurs in a two step process. The first step between 300 °C and 480 °C corresponding to a weight loss of 89 wt % can be assigned to the release of NH_3, H_2O, CO_2 and caprolactam as main products [11]. The second step (480-600°C) corresponds to the decomposition in air of the char formed during the first step. The curves of PA6 and PA6+NC are very similar, indicating again that the presence of nanoparticles does not modify the thermal stability of PA6. The fire retarded formulations, in contrast, present three main steps of degradation. Between 250 °C and 480 °C (two first steps of degradation) the materials are less thermally stable than PA6 but then between 480 °C to 670 °C (third step) a much higher residue is maintained for both intumescent formulations with and without clay. It seems that more carbonaceous residue is formed during the earlier stage of degradation and that the decomposition of the formed residue in air is slower than for pure PA6. The incorporation of nanoparticles in the PA6+OP1311 formulation improves the char strength..

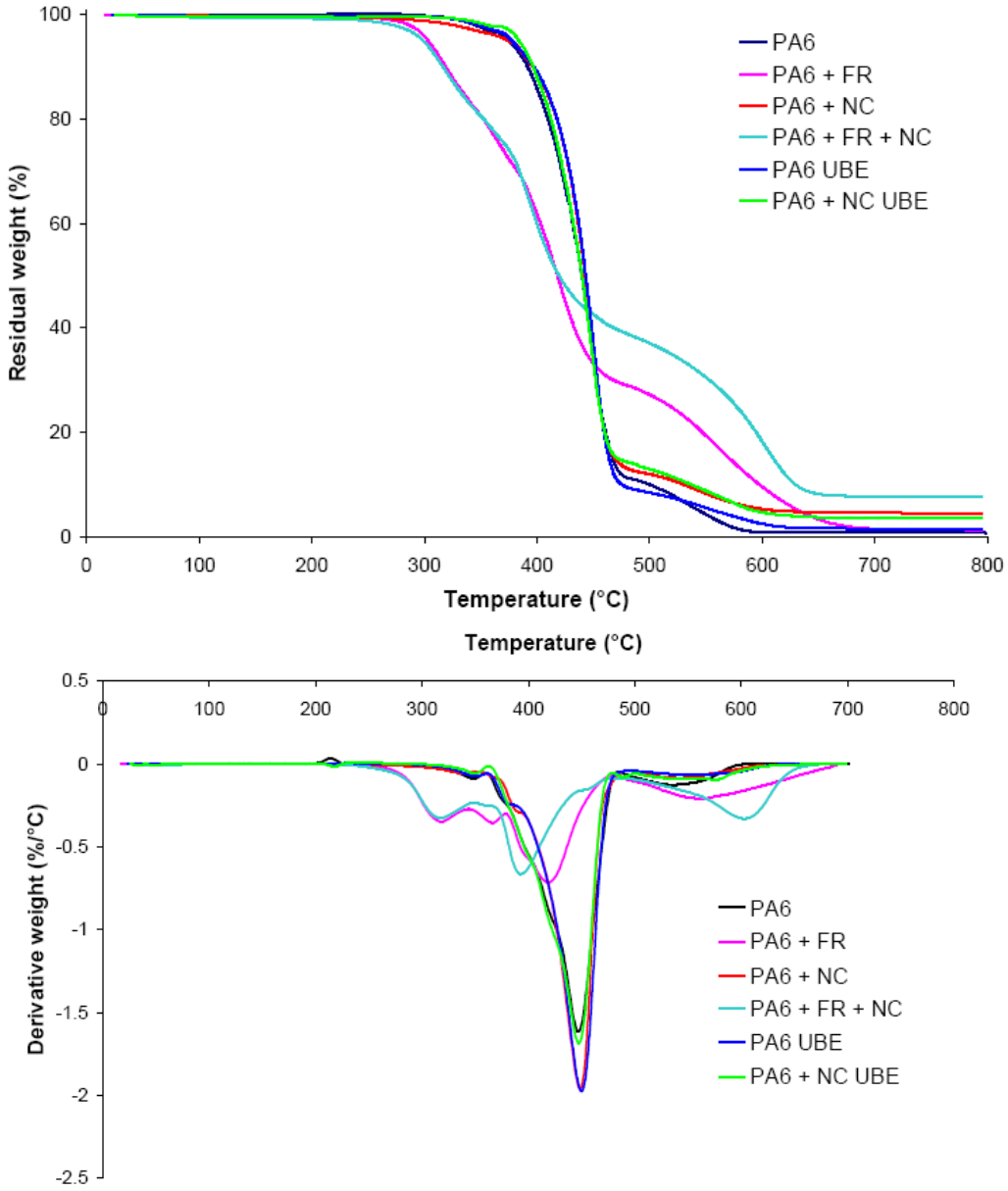

Figure 6. TG/DTG curves of PA6, PA6+NC, PA6+FR and PA6+FR+NC in air.

3.3.3 TG/FTIR for gas analysis

The TG apparatus was coupled with a Thermo Nicolet NEXUS 470 FTIR using a custom made connection. The TG/FTIR setup involved a modification of the glassware, allowing the heated transfer line from FTIR to be extended through an open fitting in the enclosed glassware. This setup allowed sampling of gases just above the degrading sample. The gas cell had a volume of 49 cm^3 and 17 cm optical path length. In order to limit the effect due to condensation, the 1.0 m long transfer line was heated to 200 °C, while the TGA interface was heated to 240 °C. FTIR measurements were carried out in a wavelength range of 4000-400 cm^{-1}, with 16 scans and resolutions of 4 cm^{-1}.

The specific gas profiles were obtained by integrating over the wavelength as a function of time. The results of H_2O, CO_2, ammonia (NH_3), and hydrogen cyanide (HCN) in nitrogen are shown in Figure 7, while those in air in Figure 8. For comparison purpose, all values were normalised by the total mass loss in the TGA. The specific evolved gas profiles of different gases in nitrogen are very similar for different materials, except that a much higher production of CO_2 is observed for PA6 and

a decrease of HCN production is found for PA6+FR+NC. On the other hand, the specific evolved gas profiles in air are quite different for different materials. Noticeably, the FR contained materials yield less H_2O and HCN. For CO_2, there appears a shift of the peak values for the FR containing materials, indicating that in the second step the degradation of the FR produces a lot of carbon dioxide. This is consistent with the finding in Figure 7 that there is a drastic increase of production of CO_2 compared to H_2O. Another important observation is that the FR reduces considerably the production of CO in the first step, although it does promote CO in the second step. Finally the FR containing materials have slightly higher NH_3 production than non FR materials.

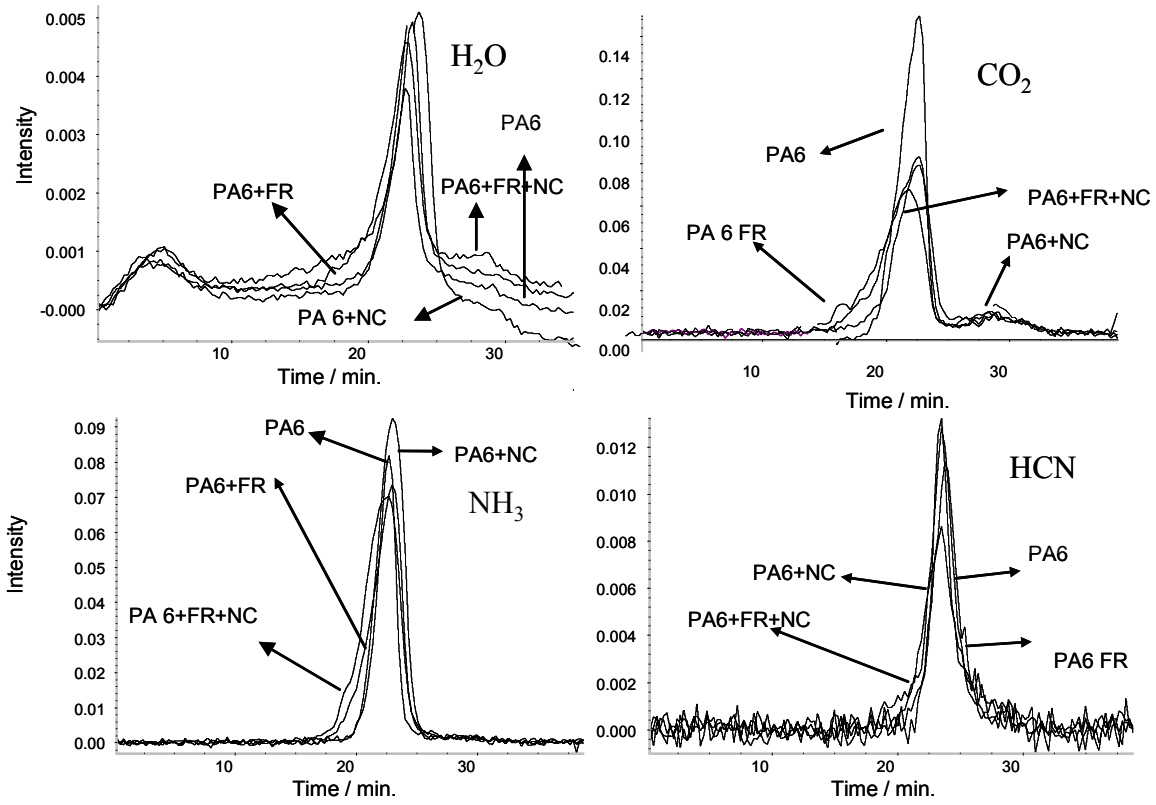

Figure 7. TG/FTIR - Specific evolved gas profiles of H_2O, CO_2, NH_3, and HCN in nitrogen

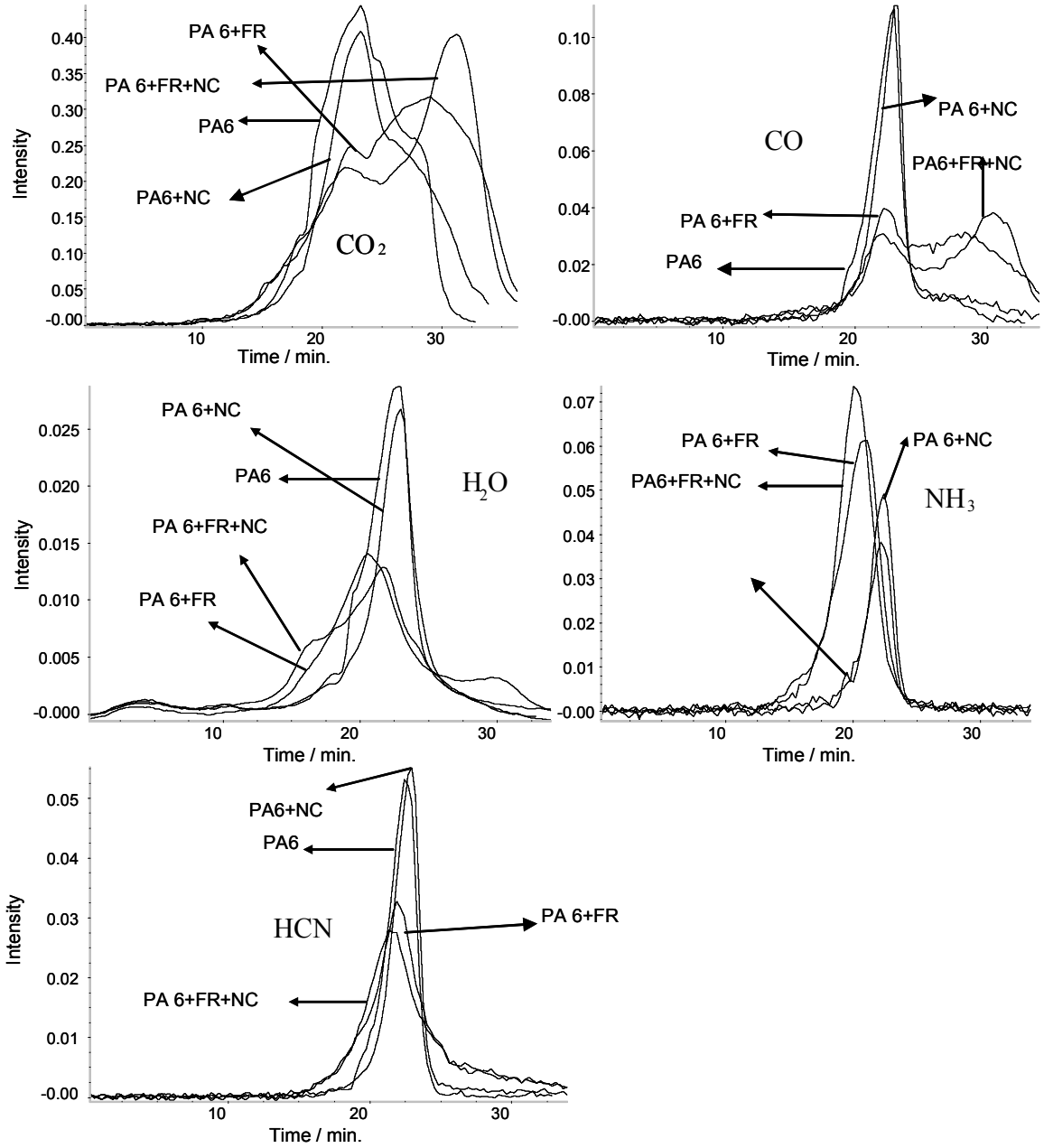

Figure 8. TG/FTIR - Specific evolved gas profile of CO2, CO, H_2O, NH_3, and HCN in air.

In Table 3, the total gas evolved for different species was obtained by integrating the instantaneous values in time. In nitrogen, the amount of H_2O evolved increases with the inclusion of the nano clay when PA6 is compared to PA6+NC and PA6+FR with PA6+FR+NC. This is likely caused by the liberation of water from the clay. The same trend is observed for NH_3 while the opposite trend is apparent for CO_2. In the case of PA6+FR+NC the increase in NH_3 might be partly caused by the evolution of water and consequent hydrolysis of the triazine ring, which in subsequent steps produces cyanuric acid and finally ammonia and carbon dioxide. The decreased levels of CO_2 might be related to a difference in the degradation pathways and possibly trapping of hydrocarbons and production of an aromatic char structure [12]. In air the fractions will depend on oxidation reactions. The increased amounts of CO_2 produced by the fire retardant samples are believed to be a function of degradation of the intermediate char at higher temperatures. Also the FR does not contribute to significant increase of HCN either in N_2 or air.

Table 3. TG/FTIR - Total integrated (absorption) values of the specific gas profiles in nitrogen and air atmospheres.

Atmosphere	Gas	Wave number range /peak cm^{-1}	Baseline cm^{-1}	Integrated values/mass loss			
				PA6	PA6+ NC	PA6+ FR	PA6+FR +NC
N_2	H_2O	1507	1500-1520	0.08	0.11	0.12	0.14
	CO_2	661-675	661-675	2.55	1.71	2.21	1.81
	NH_3	3315-3341	3315-3341	1.02	1.59	1.42	1.75
	HCN	710-715	710-715	0.11	0.12	0.11	0.12
Air	H_2O	1507	1500-1520	0.76	0.65	0.56	0.75
	CO_2	661-675	661-675	23.5	22.2	29.0	29.0
	NH_3	3315-3341	3315-3341	0.62	0.82	1.62	1.83
	HCN	710-715	710-715	0.84	0.89	1.06	1.04
	CO	2030-2142	2030-2142	2.07	2.05	2.44	2.50

The main findings of the TG/FTIR study are:

1. The TGA results indicate that the curves for PA6 and PA6 + NC depict one step degradation whereas PA6 + FR and PA6 + FR + NC show two stage decomposition process under nitrogen. The inclusion of nanoclay alone does not alter the thermal degradation of PA6 apart from its influence on increased char (residual mass) formation. On the other hand, FR changes the degradation behaviour by lowering the degradation temperature in PA6 + FR and PA6 + FR + NC composites. It is observed that a lot of FR goes to the gas phase as diethylphosphinic acid.
2. All the composites (PA6, PA6 + FR, PA6 + NC and PA6 + FR + NC) show a two-step decomposition process, the second step degradation step is due to transient char formation.
3. The main gases evolved from PA6 and PA6 + NC in nitrogen are ε-caprolactam, hydrocarbons, carbon dioxide, water and ammonia. Other composites namely PA6 + FR and PA6 + FR + NC evolve the same volatiles with an additional phosphorous containing species. PA6 + FR yields diethylphosphinic acid (from aluminium diethylphosphinate), and the water and carbon dioxide arise from the decomposition of melamine polyphosphate through condensation and hydrolytic decomposition.
4. The products of thermo-oxidative are carbon monoxide, carbon dioxide, water and hydrogen cyanide for all the composites. The second major degradation step, as observed by TGA in air, produces mainly carbon dioxide. In comparison with results under nitrogen peaks due to ε-caprolactam and hydrocarbons are less in strength since the oxidation disrupts them and fragmenting them into carbon dioxide and water.
5. The yield of toxic gas namely the hydrogen cyanide does not increase when phosphinate FR is used.

3.3.4 TG/ATR for (PBT) for the structure of condensed phase

Whilst the condensed phase analysis of the residue (by FTIR-ATR) of PA6 is ongoing, we present the results of TG/ATR for PBT modified by a phosphinate FR or nanoparticles (sepiolite) or the combination of phosphinate and nanoparticles.

The samples from the TGA tests were taken out at different temperature, 25 °C, 330 °C, 360 °C, 390 °C and 450 °C, and analysed by FTIR-ATR. The FTIR-ATR spectra of the sample at 25°C (virgin material) and its residue at 450°C are shown in Figures 9a-d for PA6, PA6+NC, PA6+FR, and PA6+NC+FR respectively.

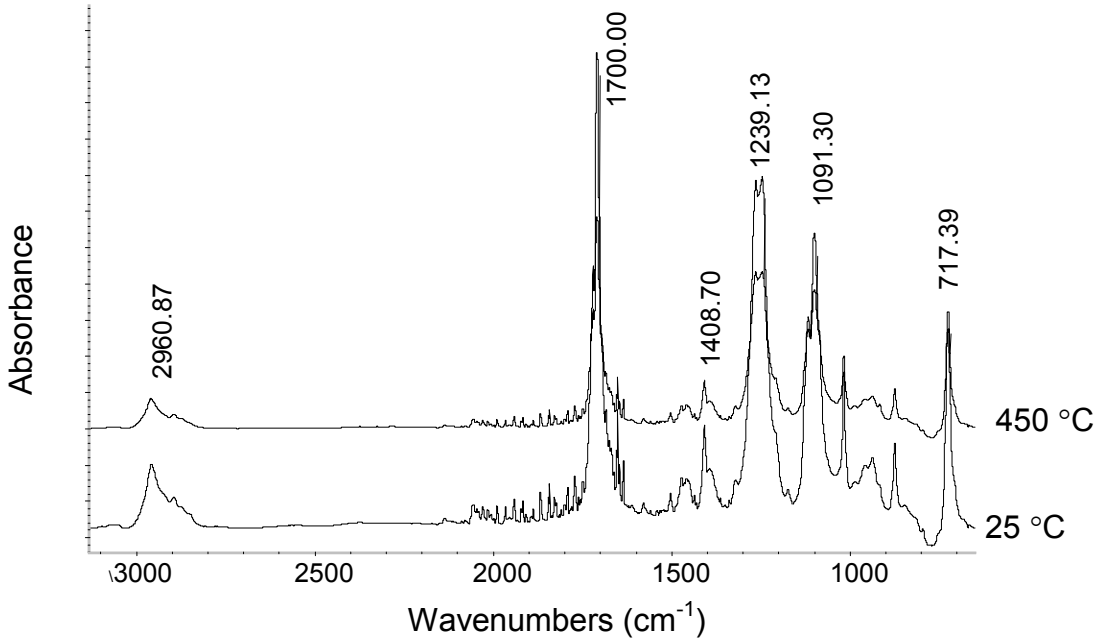

Figure 9a. FTIR (ATR) spectra of PBT at 25 °C, and its solid residue at 450 °C

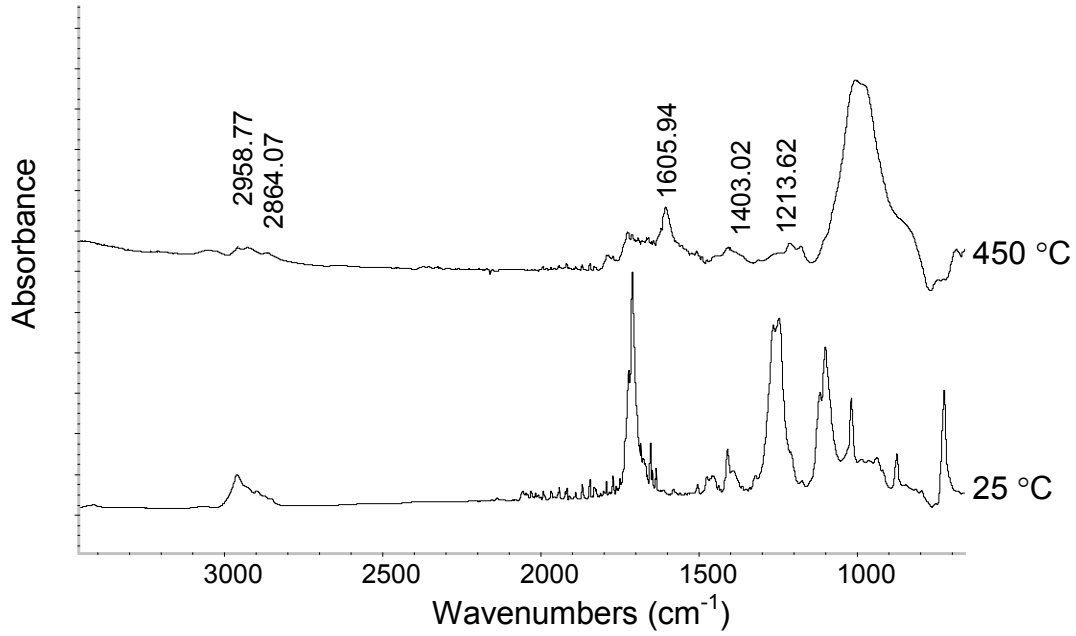

Figure 9b. TG/ATR - Spectra of PBT+NC at 25 °C, and its solid residue at 450 °C

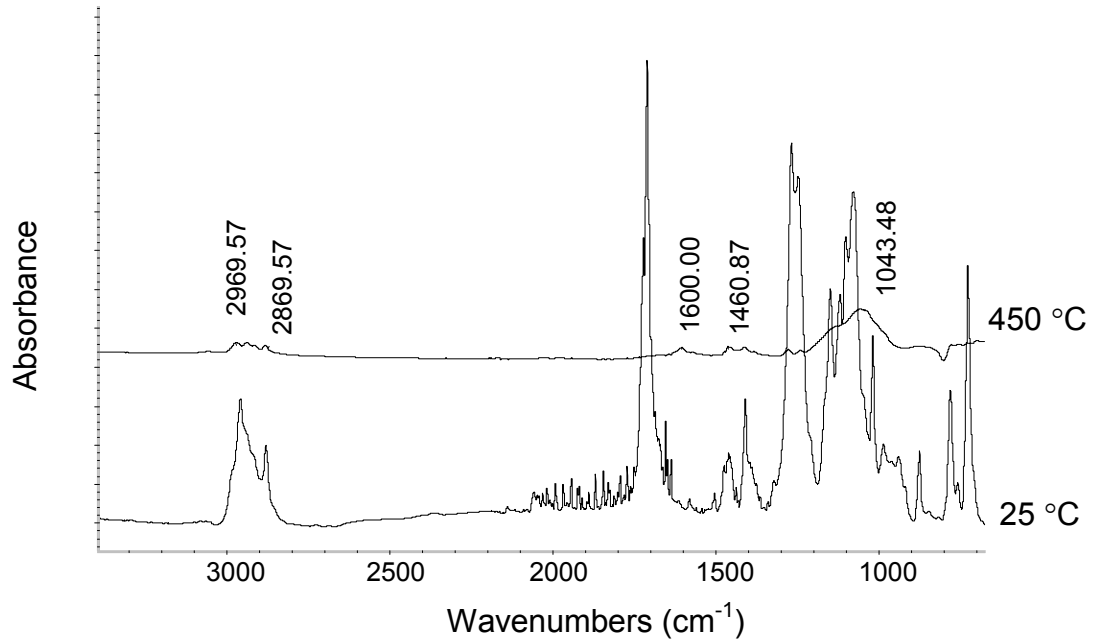

Figure 9c. TG/ATR - spectra of PBT+FR at 25 °C, and its solid residue at 450 °C

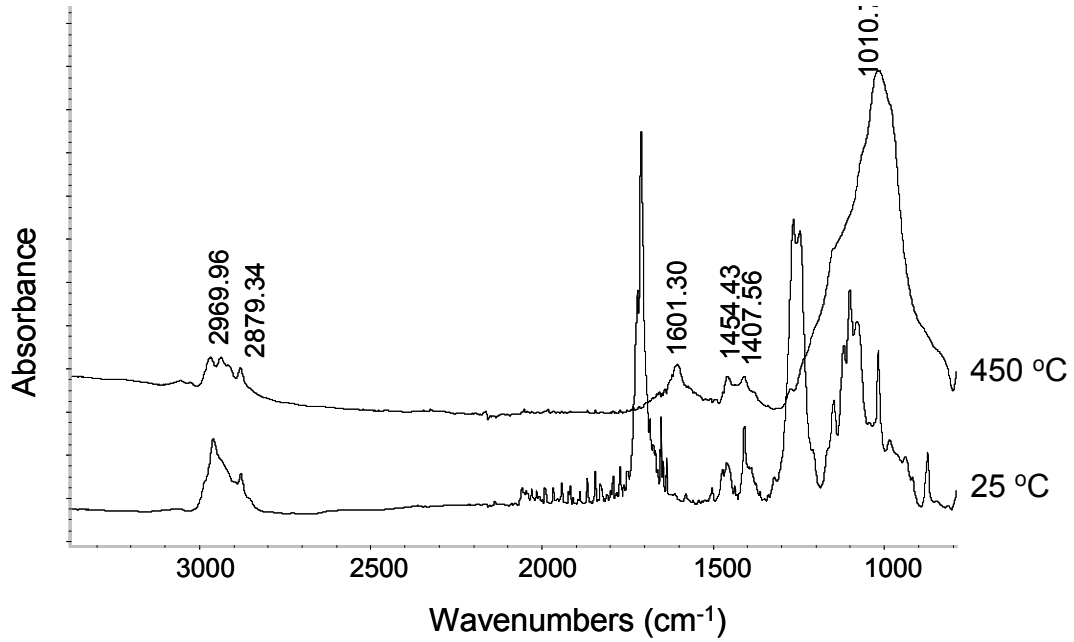

Figure 9d. TG/ATR - spectra of PBT+NC+FR at 25 °C, and its solid residue at 450 °C

Figures 9a-d show that both the phosphinate FR and the nanoparticles change the structure of char compared with pure PBT. In contrast to the pure polymer which leaves a char consisting of oligomeric components of PBT, the fire retarded polymer (by phosphinate and /or nanoparticles) leaves a char consisting of polycyclic aromatic hydrocarbons (PAH). The PAH structure of the char is expected to make the char stronger and capable to withstand erosion in full scale fire tests. This observation is verified from the strength analysis of the char residue in intermediate scale flammability experiments such as those in the cone calorimeter, where char is formed behind the flames in the absence of oxygen. The main findings of the TG/ATR test are:

- The char at 450 °C for PBT is an oligomeric component whereas the char from PBT+FR and PBT+NC formulations comprise aluminium phosphinate and sepiolite respectively along with polycyclic aromatic hydrocarbons. Specifically, the char from the formulation

PBT+FR+NC consists of aluminium phosphinate, sepiolite and polycyclic aromatic hydrocarbon with alkyl groups attached.

- During the degradation process FR interacts chemically with PBT and degrades to ethylene and aluminium phosphinate. Above 390 °C aluminium phosphinate reacts chemically with PBT. In contrast, the grafted organic molecule degrades from NC leaving behind the sepiolite network and the NC acting catalytically with PBT (See discussion in section 3-4).
- The char from PBT+FR+NC would be stronger than the char from pure PBT, because PBT upon degradation produces only the oligomers. The PAH structure of the char is expected to make the char stronger and capable of withstanding erosion in full scale fire tests. This observation is verified from the strength analysis of the char residue in intermediate scale flammability experiments such as those in the cone calorimeter, where char is formed behind the flames in the absence of oxygen.

4. Mesoscale experiments and measurements

4.1 Tube Furnace

4.1.1 Experimental details

The fire toxicity of each material has been measured under different fire conditions. The influence of polymer nanocomposite formation and fire retardants on the yields of toxic products from fire is studied using the ISO 19700 steady state tube furnace, and it is found that under early stages of burning more carbon monoxide may be formed in the presence of nanofillers and fire retardants, but under the more toxic under-ventilated conditions, less toxic products are formed. Carbon monoxide yields were measured, together with hydrogen cyanide (HCN), nitric acid (NO) and nitrogen dioxide (NO_2) yields for PA6 materials, for a series of characteristic fire types from well-ventilated to large vitiated. The yields are all expressed on a mass loss basis.

4.1.2 Results and discussions

Figure 10 shows the CO yields from the PA 6 based materials under different fire conditions. This shows consistently lower CO yields for well-ventilated burning compared with small or large under-ventilated conditions [13]. Under well-ventilated conditions it shows increased CO yields for materials including nanoclay or a fire retardant, but surprisingly the combined effect of both FR and NC result in lower CO yield. Under the more toxic under-ventilated conditions, overall the yields of CO are much higher, but there is little difference between small and large under-ventilated conditions, or on incorporation of either fire retardant or nanoclay [13].

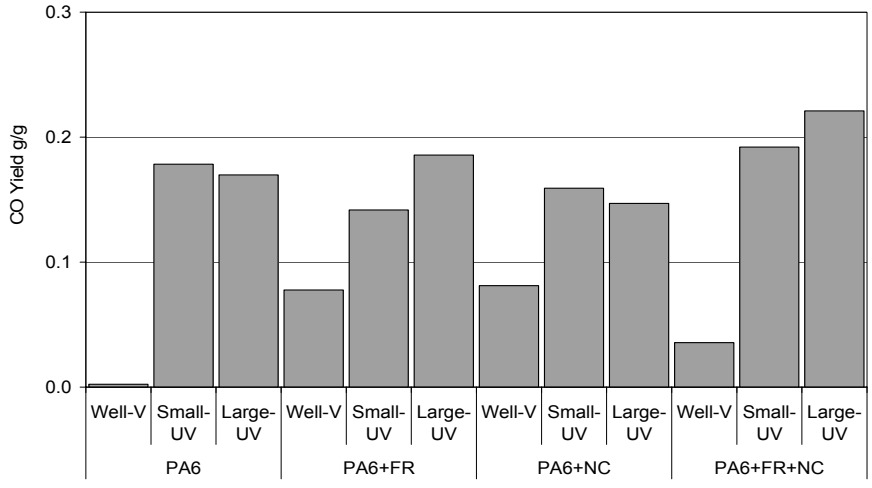

Figure 10. Carbon monoxide yields for PA 6 based materials in tube furnace

A similar trend to carbon monoxide is observed for PA6 for hydrogen cyanide. HCN yields increase with reduced ventilation, but is less sensitive to the furnace temperature. The NO_2, NO and HCN yields are presented in Figure 11.

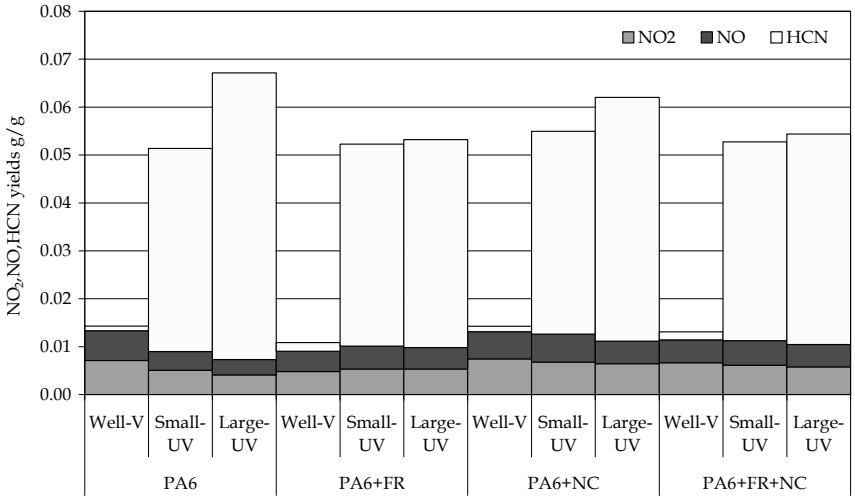

Figure 11. HCN, NO2, and NO yields for PA 6 based materials in tube furnace

The higher yield of HCN for PA6+FR, for well-ventilated flaming corresponds to a higher yield of CO for the same conditions. It is interesting to note that the HCN yield increases with severity of the fire condition, whereas the CO yield levels off or even decreases. Results are consistent with the TGA/FTIR data presented in Table 3, section 3.3.3.

4.2 Cone calorimeter

4.2.1 Experimental details

Slab samples having dimensions of 100×100×6 mm were manufactured by extrusion at CDCMP in Italy. A summary of the compositions and physical properties of the PA6-based materials for the Cone tests is listed in Table 4.

Table 4. Composition and physical properties of PA6-based materials.

	PA6	PA6/NC_UBE	PA6/NClois ite	PA6/FR	PA6/NC/FR
Mass (g)	65.3	66.5	66.8	69.2	69.0
ρ (kg/m^3)	1129	1137	1137	1185	1177
PA6 (%)	100	97.5	95	82	77
NP (%)	-	2.5	5	-	5
FR (%)	-	-	-	18	18

Prior to the tests, all the samples were dried in a vacuum oven at 80˚C for at least 72 hours to minimise the moisture effect and then transferred to a desiccator. Measurements were carried out on a cone calorimeter provided by the Dark Star Research Ltd, UK. In order to minimise the conduction heat losses to insulation and to provide well-defined boundary conditions for numerical analysis of these tests, a sample holder was constructed as reported in [14] with 4 layers (each layer

is 3mm thick) of Cotronic ceramic paper at the back of the sample and 4 layers at the sides. A schematic view of the sample holder is shown in Figure 12. Three external heat fluxes (40, 50 and 60 kW/m^2) were used with duplicated tests at each heat flux.

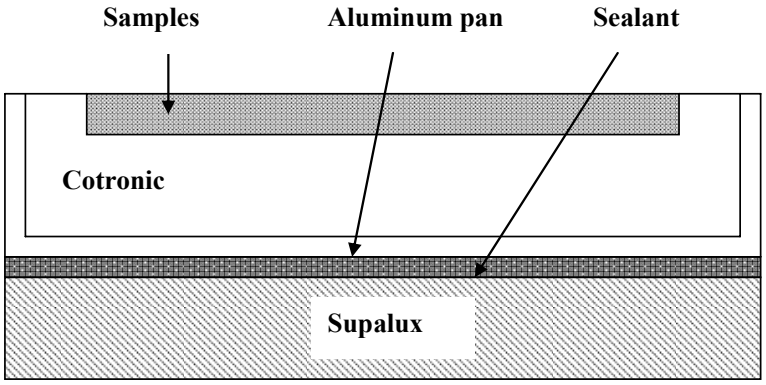

Figure 12. A schematic view of the sample holder used in Cone calorimeter tests.

4.2.2 Results and discussions

Ignition times

The ignition time for each test, in which a constant heat flux was impinging on the sample, was obtained by examining the second derivate of the mass loss data and/or the first derivative of the heat release rate data. Both methods yield similar results after the time delay for transporting the hot gas to the HRR analyser in the hood is accounted for. A summary of the ignition time for all the tests conducted is presented in Figure 13, where for duplicated tests the final ignition time is taken as the average of two tests. Ignition appears to occur earlier with nanoclay with similar results reported in [15] for a different PA6 nanocomposite. It should however be pointed out that there is no general conclusion with regard to the effect of nanoclay on ignition of polymers, because both delaying and accelerating ignition by nanoclay have been noted in the literature as well as in the PredFIRE project.

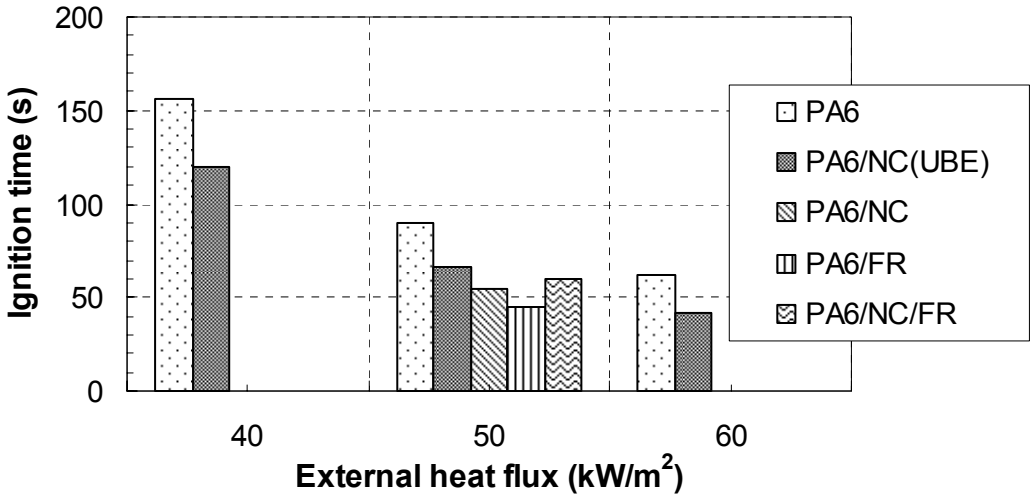

Figure 13. Experimental ignition time of PA6 based materials at different heat fluxes.

Mass loss rate

The Savitzky–Golay (SG) smoothing algorithm developed in [16] was used in this work to smooth the mass loss data. The smoothed mass loss rate for PA6/NC(UBE) at different heat fluxes are

shown in Figure 14 together with those for pure PA6 obtained under the same test conditions. It is seen that nanoparticles have a negligible effect prior to the first peak MLRs and the reduction at the steady burning stage is also moderate about an average of 15%. However the second peak MLRs observed for pure PA6 due to the back side effect, which occurs when the material throughout has a uniform temperature as a result of heat accumulation at the insulated back, is essentially removed by addition of 2.5 wt. % nanoparticles. These results seem to indicate that the fire retardancy effect of the surface layer increases as the pyrolysis process progresses because the depth of the surface layer increases with more nanoparticles accumulated on the surface.

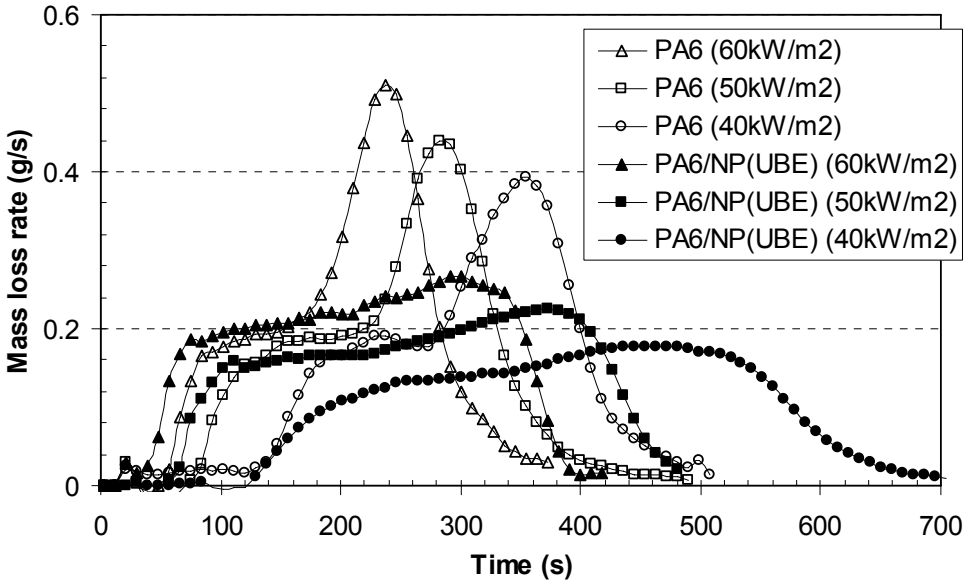

Figure 14. Comparison of the mass loss rate history of PA6 and PA6/NC(UBE) at different heat fluxes (sample thickness is 6mm).

To examine the effect of thickness, tests were carried out for 6mm, 12mm and 24mm samples at 50kW/m^2, for which the results for PA6 and PA6/NC(UBE) are compared in Figure 15. For a 12mm PA6 sample the steady burning MLR is almost constant, about 0.19g/s. A plateau shows typical behaviour of thermally thick materials. Although there is a significant reduction of the second peak MLRs by PA6/NC(UBE), the reduction of the MLRs at the steady burning stage is, however, moderate, only about 25%.

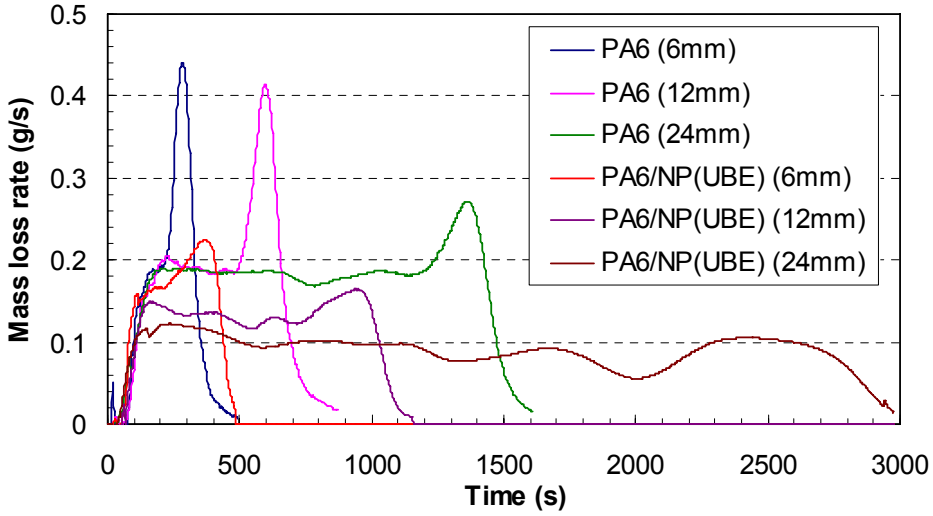

Figure 15. Comparison of the mass loss rate for PA6-based materials at different sample thicknesses at 50kW/m^2.

Heat release rate

Figure 16 shows a comparison of the heat release rate (HRR) of PA6 and PA6/NC(UBE) at different heat fluxes. As the HRR is proportional to the MLR, the proportional factor being the heat of combustion, the HRR results have similar trends to those in the MLR. Significant reduction of the second peak HRRs was achieved by the nanocomposite.

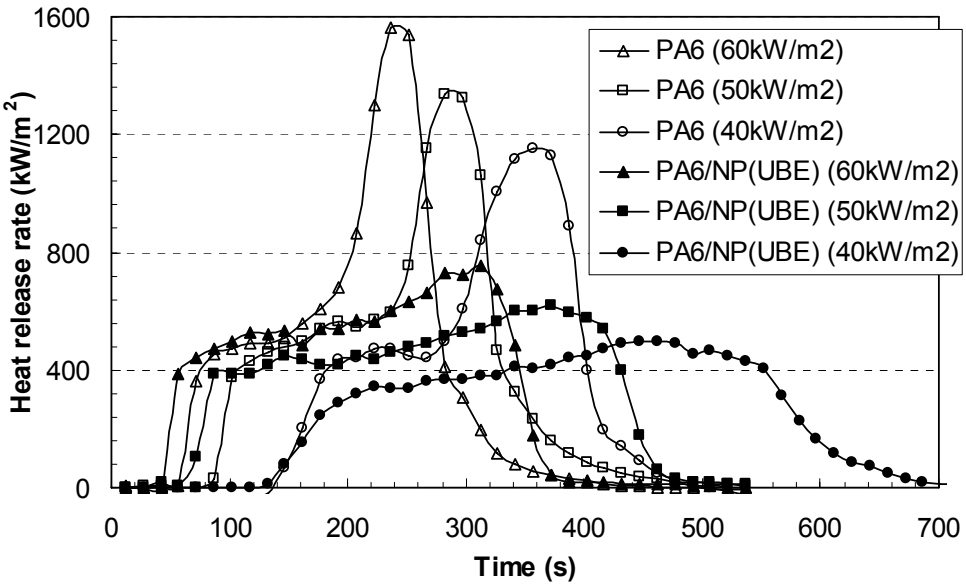

Figure 16. Comparison of the heat release rate of PA6 and PA6-nano at different heat fluxes (sample thickness is 6mm).

A comparison of the HRR of PA6, PA6-nano, PA6/FR and PA6/NP/FR is presented in Figure 17. The FR reduces the HRR more substantially compared to the NC, but it is worth noting that the FR concentration 18 wt. % compared to 2.5 and 5 wt. % of NC. Although PA6/NC/FR has the lowest HRR, with a reduction of 70% in comparison to pure PA6, it shows only marginal improvement over PA6/NC.

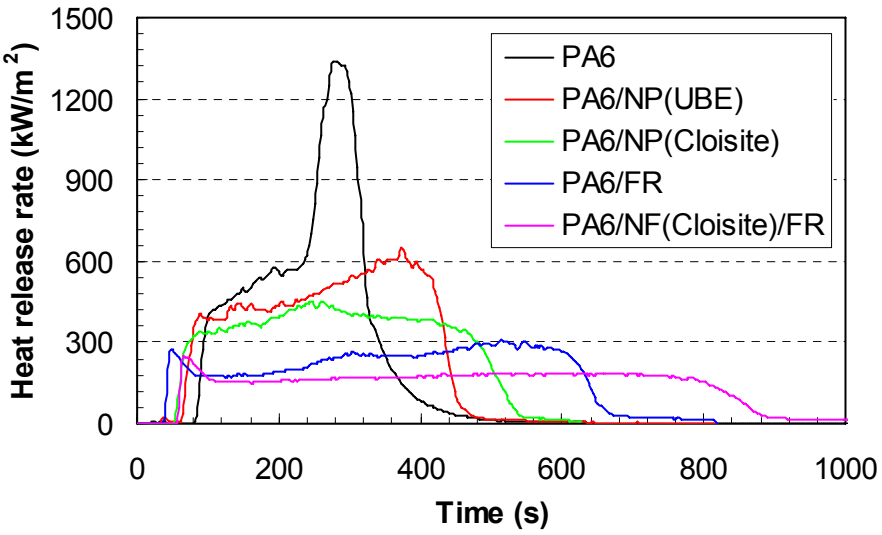

Figure 17. Comparison of the HRR of PA6 and PA6/NC(UBE), PA6/NC PA6/FR, and PA6/NC/FR at 50kW/m^2 (sample thickness is 6mm).

Effective heat of combustion

Figure 18 presents a comparison of the effective heat of combustion, calculated as the ratio of the total heat release (THR) to the total mass lost (TML), for all the formulations. An average value of 26.5 ± 1 kJ/g was observed for all tests with PA6, PA6/NC, and PA6/NC(UBE). For PA6/FR and PA6/NC/FR the EHC is significantly smaller – 21kJ/g for PA6/FR and 19kJ/g for PA6/NC/FR. Like most phosphorus fire retardants char formation is the main chemical (cross linking) mechanism [17].

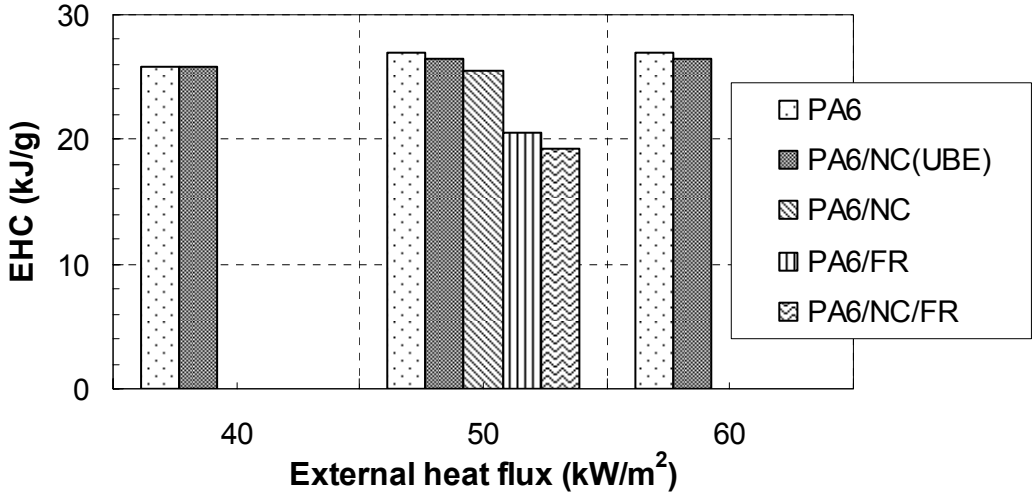

Figure 18. Comparison of effective heat of combustion for PA6-based materials at different heat fluxes.

Smoke, carbon monoxide, and carbon dioxide production

Figures 19-21 present respectively smoke, carbon monoxide and carbon dioxide yield for all the PA6-based materials. Pure PA6 generally produces the lowest smoke and carbon monoxide, while PA6/NC and PA6/NC(UBE) yield slightly higher values. This is one of the main advantages of nanocomposites as they do not result in increasing production of smoke and toxic gases in comparison to most fire retardants. It is important to note that adding FR (both PA6/NP and PA6/NC/FR) results in much higher smoke and carbon monoxide production. For smoke and carbon monoxide the increase is by a factor of 3 and 10 respectively. In terms of carbon dioxide production, there is no distinctive difference between all formulations, though FR contained materials seem to have less production of CO_2.

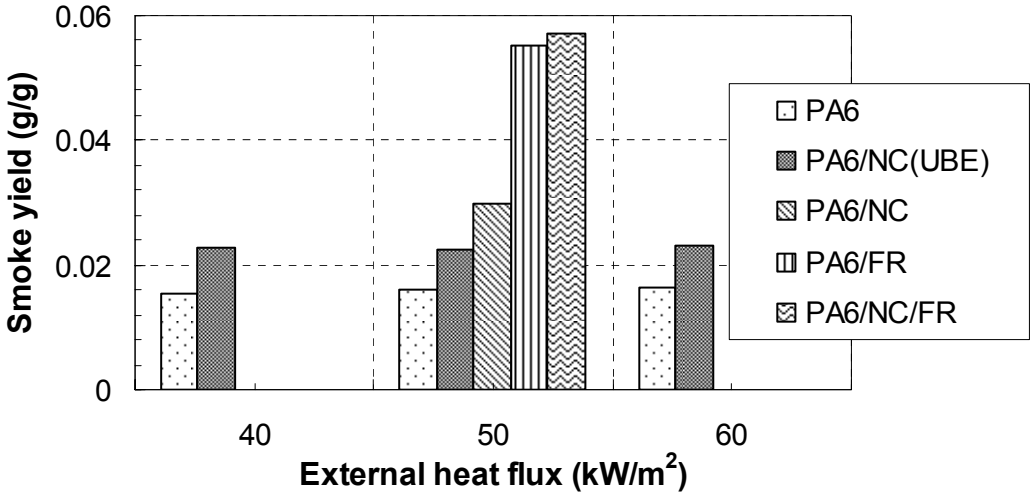

Figure 19. Comparison of smoke yield for PA6-based materials at different heat fluxes.

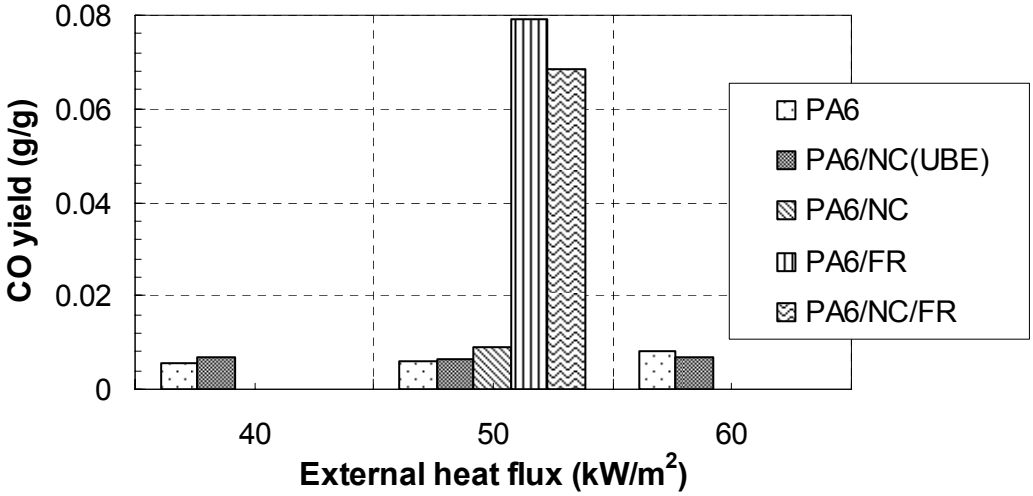

Figure 20. Comparison of carbon monoxide yield for PA6-based materials at different heat fluxes.

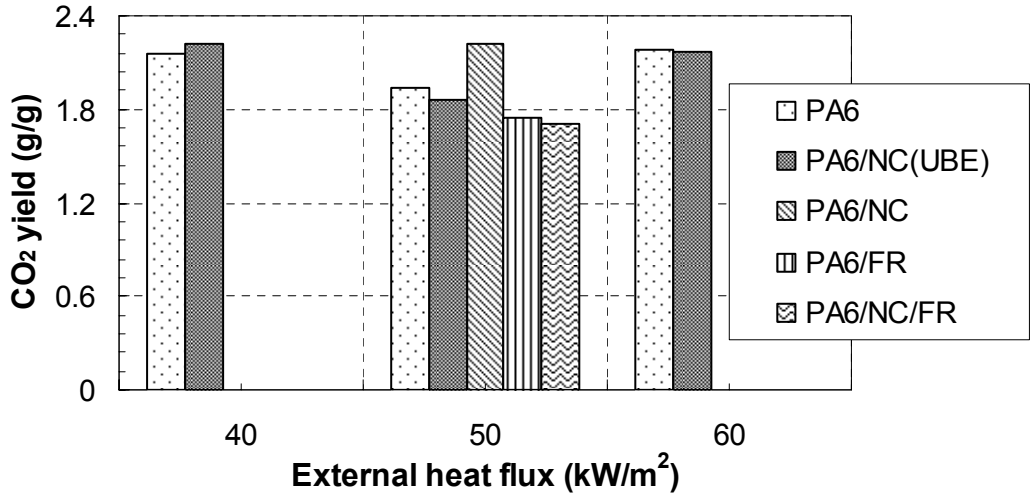

Figure 21. Comparison of carbon dioxide yield for PA6-based materials at different heat fluxes.

4.3. UFA (Universal Flammability Apparatus)

4.3.1 Experimental details

The universal flammability apparatus (UFA) shown in Figure 22 has a controlled oxidizer atmosphere and representing burning on a 100 mm diameter sample in horizontal orientation in a more realistic way than the standard cone calorimeter. Tests were conducted in over-ventilated fires but at reduced oxygen concentration (15, 17.5 and 21 %) in the oxidizer stream. Because of in-depth absorption of the sample under infra-red radiation, samples with and without a layer of carbon black coating were tested.

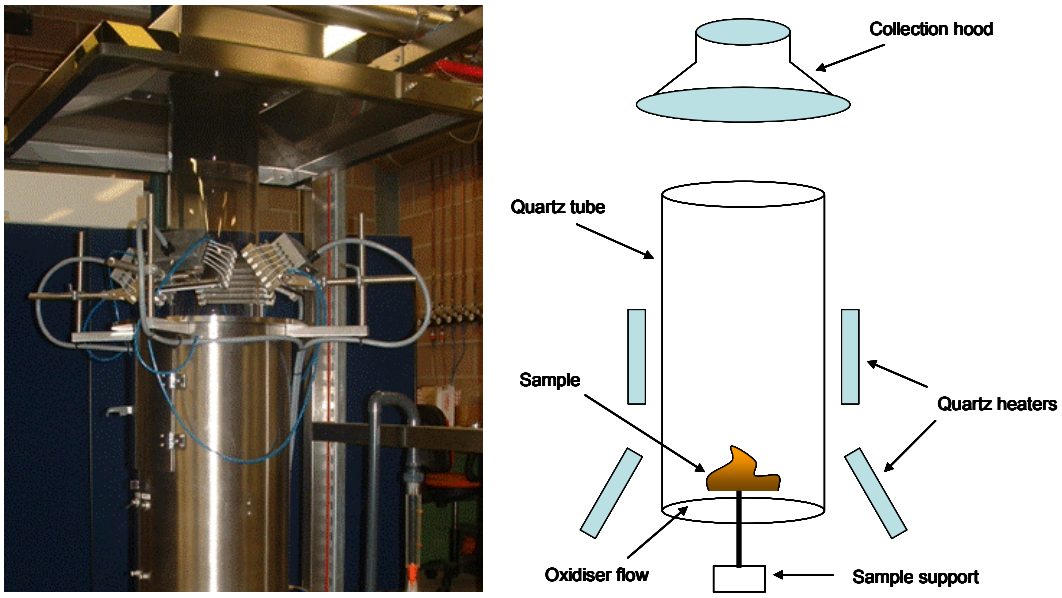

Figure 22. The universal flammability apparatus (UFA) (left) and a schematic view of the UFA (right).

4.3.2 Results and discussions

Figure 23 shows a comparison of the CO yield and CO/CO_2 ratio for PA6 samples w/wo carbon black coating. Both CO yield and CO/CO_2 ratio increases with reduced oxygen concentration. Results on under ventilated conditions were not yet available during the preparation of this report.

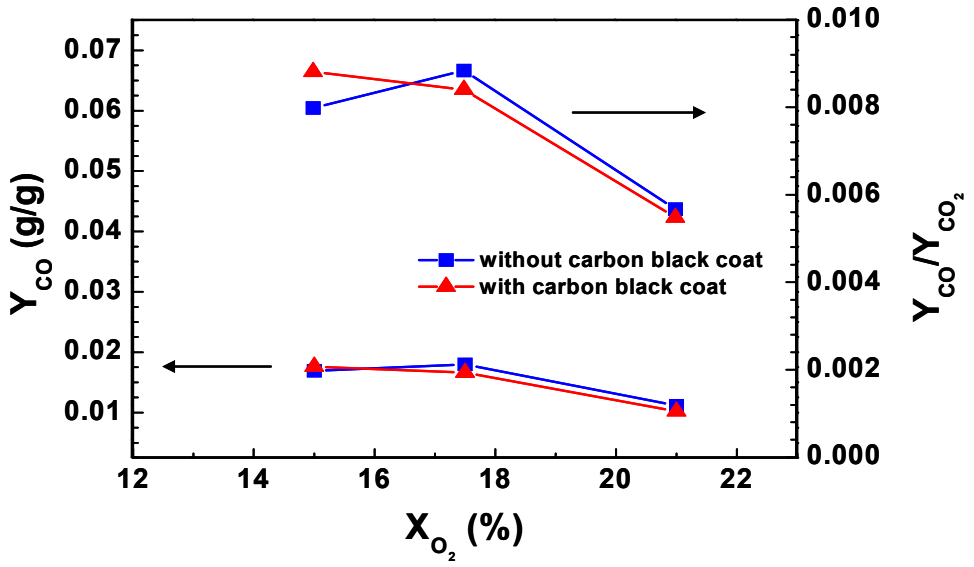

Figure 23. Carbon monoxide yield and CO/CO2 ratio for PA6 in over-ventilated fires but at reduced oxygen concentration in the oxidizer stream in the UFA apparatus

5. Numerical prediction of polymer behavior in the cone using TGA measurements in Nitrogen

This section shows how the kinetic parameters, namely the pre-exponential factor and activation energy that can be derived from the TGA measurements of a PA6 sample are used in a numerical model to predict the surface temperature history and mass loss of the sample with finite thickness in the cone calorimeter.

5.1 Kinetic parameters in the TGA

Figure 24 shows the TGA measurements of a PA6 sample in nitrogen (represented as symbols) at five heating rates, i.e. 1, 2, 5, 10 (also shown in Fig. 4) and 20 K/min, along with the best fits (represented as lines) obtained using a first-order reaction mechanism, i.e.

$$\frac{dX}{dt} = (1 - X) A_r e^{-\frac{E}{RT}} \qquad (1)$$

where X is the fraction of the mass lost; t is time; A_r is the pre-exponential factor; E is the activation energy; R is the universal constant; and T is the temperature of the solid. The derived optimal values for E and log(A_r) are 196.4 kJ/mol, and 11.988s^{-1} respectively.

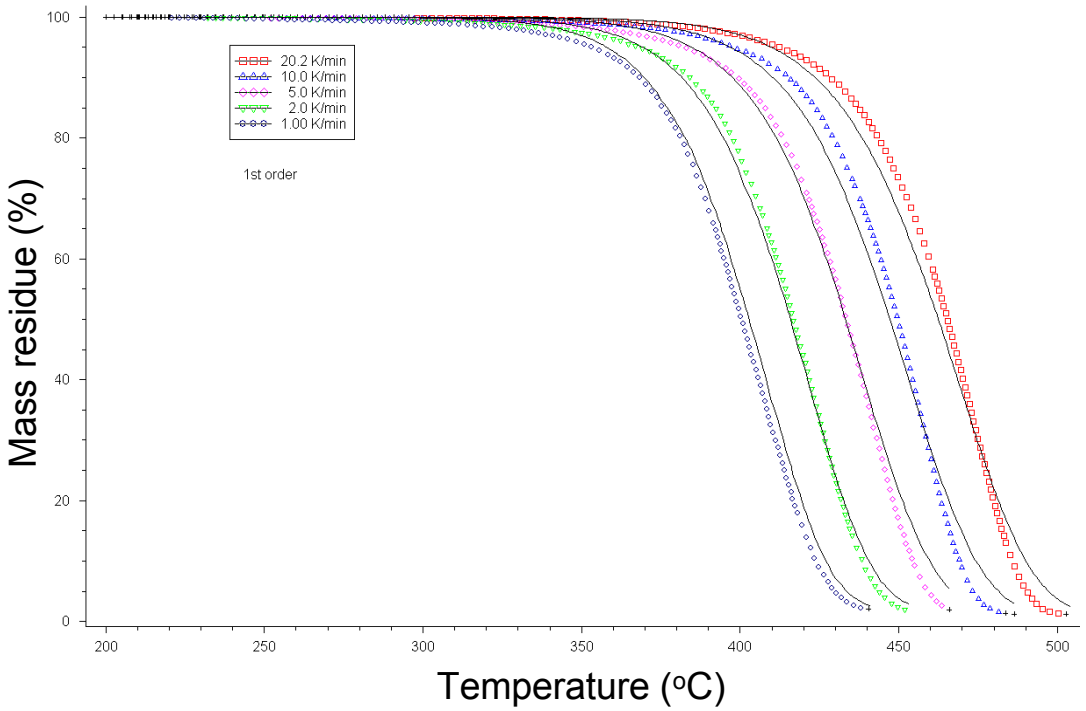

Figure 24. TGA Degradation of PA6 in nitrogen at different heating rates. Symbols denote experimental data and lines are the best fits from the model using one-step reaction mechanism.

5.2.1 Predicted surface temperature history in the cone for TGA obtained pyrolysis rate (Eq. 1)

The Arrhenius expression (Eq. 1) using the activation energy and pre-exponential factor derived from TGA measurements of a PA6 sample in N_2 was incorporated in a standard 1D pyrolysis model described in Section 6. The thermal properties used in the model are the ones from the ignition tests (4.2.2) as described in section 6 in conjunction with the MDSC experiments (3.2.2). Figures 25a-c show the predicted surface temperature histories for thermally intermediate (6mm) and thick (12mm) conditions at 20, 40 and 60kW/m^2 respectively. It is shown that the main pyrolysis process occurs nearly at a constant temperature. However, the predicted steady state surface temperature appears to be dependent on external heat flux, increasing from 415^{o}C at 20kW/m^2 to 450^{o}C at 40kW/m^2 and 480^{o}C at 60kW/m^2. The ignition temperature for pure PA6 derived from the ignition tests (described in Section 6) has a value of 715K (442^{o}C), well in the range of the results shown here. Thus the thermal model is a good accepted engineering approximation for this case.

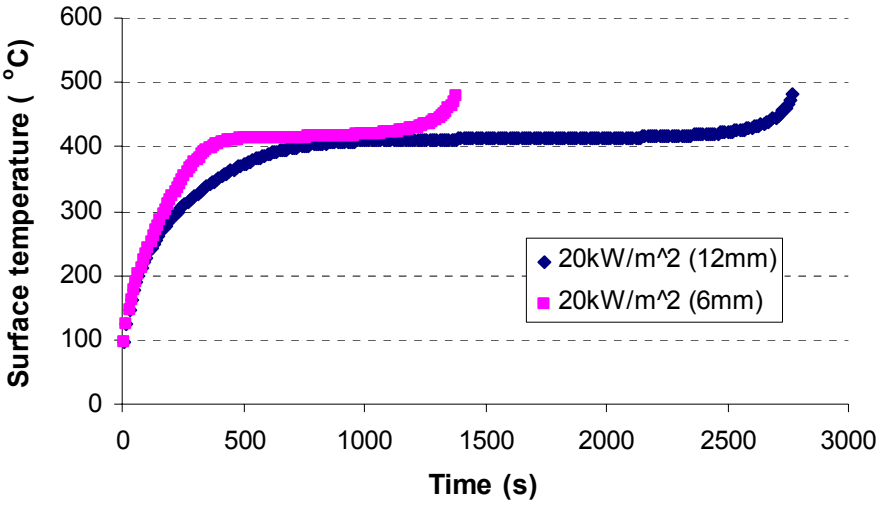

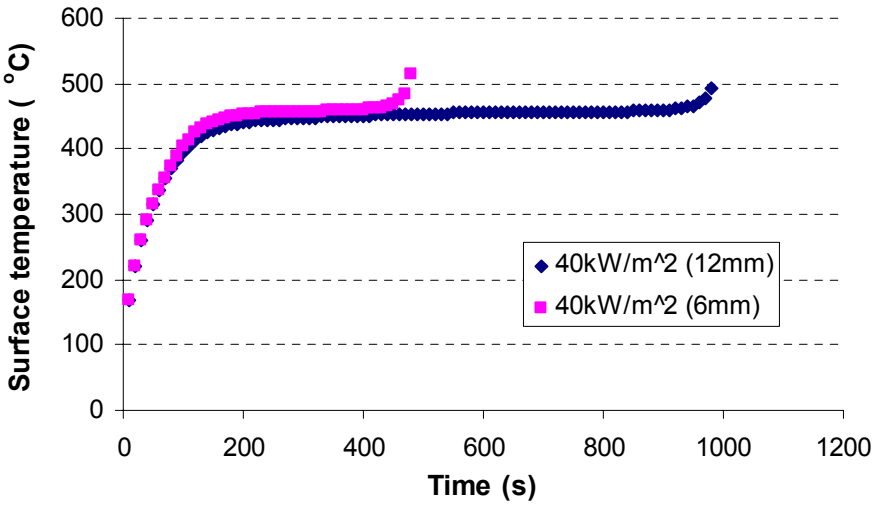

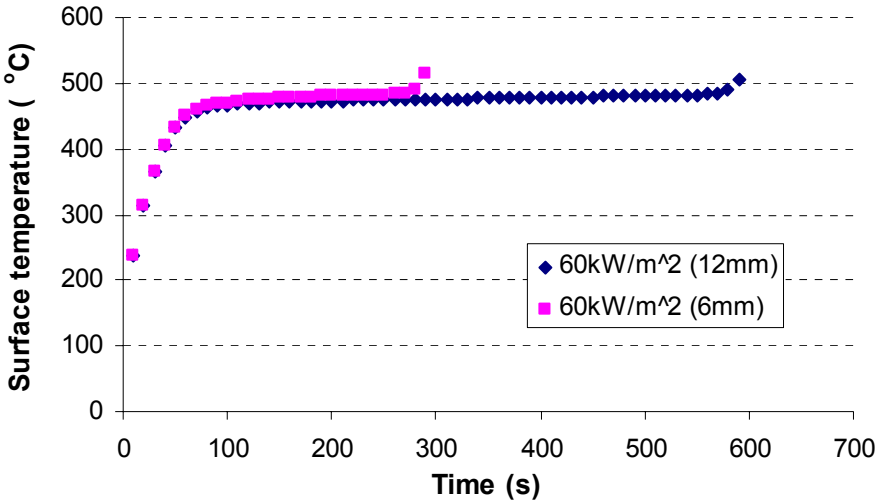

Figure 25. Predicted surface temperature histories for 6 and 12 mm PA6 samples in N_2 at: a) 20, b) 40, and c) 60kW/m2.

5.2.2 Predicted mass loss in the cone calorimeter

In Figure 26, the TGA measurements are "related" to the predictions in the cone calorimeter by plotting the surface temperature history against the normalised residual mass (the residual mass normalised to the initial mass) for 6 and 12 mm samples at different heat fluxes using the 1D model as in the previous section. It is interesting to note that sample thickness has negligible effect on the predicted surface temperature which is nearly constant except in the regions near the end of the pyrolysis process where the material becomes thermally thin. Because of the thin layer near the end of pyrolysis a similarity appears in the mass loss rate between the TGA results in Figure 24 and cone results in Figure 26, indicating that the exposed surface in the cone calorimeter pyrolyses in a similar way to the sample in the TGA. Another important observation from the present results is that the heating rates from 1-20 K/min in the TGA cover the behaviour of the polymer for the heating fluxes in the cone for the range of 20 to 60 kW/m^2.

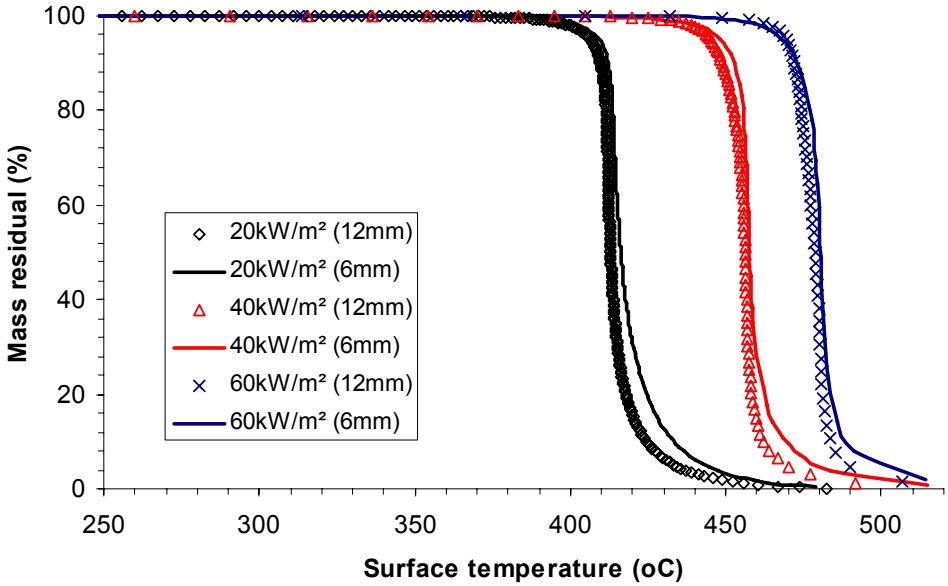

Figure 26. Predicted surface temperature using the kinetic energy and pre-exponential factor derived in the TGA against mass residue for 6 and 12 mm PA6 samples at different heat fluxes.

6. Numerical model for the pyrolysis of polymer nanocomposites

The present numerical model was developed based on a standard non-charring model using the ignition temperature concept, i.e., the surface temperature remains constant after reaching the prescribed ignition temperature until the material pyrolyses completely. The accuracy of the standard non-charring model was demonstrated by comparing model predictions with exact analytical solutions and the results generated by an integral model.

6.1. Mathematical formulations

The development of the present methodology is inspired by an analytical study for pyrolysis of charring materials [18], where it was shown that the heat flux at the char-virgin interface (with the assumption that surface absorptivity and emissivity are one) has the following form:

$$\dot{q}''_{net}(t) = \frac{d}{\delta_c + d}\left(\dot{q}''_{ext} - \sigma T_{ig}^4\right) \tag{2}$$

where δ_c is the char thickness, $\dot{q}''_{ext}$ is the external heat flux and d is a characteristic radiation length that also takes into account the change of conductivity, k_c, with temperature:

$$d = \frac{k_c\left(T_{ig}\right)T_{ig}}{4\sigma T_{ig}^4} \tag{3}$$

Here T_{ig} denotes the ignition temperature that can be determined from the ignition tests and σ is the Stefan-Boltzmann radiation constant.

Note that convection heat losses were neglected in the analyses in [18] as radiation is the dominant mode of heat losses at high temperatures.

Rearranging Eq. 2, we obtain:

$$1 + \frac{\delta_c}{d} = \frac{\left(\dot{q}''_{ext} - \sigma T_{ig}^4\right)}{\dot{q}''_{net}(t)} \tag{4}$$

Equation 4 implies that the heat flux at the char-virgin interface will decrease with increasing char depth and/or decreasing conductivity. Comparing Eqs. (2) and (4) and noting that d is a material constant, we obtain that the heat flux at the interface is a function only of the char depth δ_c.

Although burning of nanocomposites is different from that of charring materials, because for charring materials (such as wood) it can be usually assumed that the volume does not change before and after burning whereas for nanocomposites the volume can change significantly because of the small amount of nanoparticles (typically less than 5%) used, the heat transfer mechanisms are similar for both cases. Both involve formation of a surface layer (a char layer for charring materials whereas a nano layer for nanocomposies), and the thickness of the surface layer increases as pyrolysis continues. Thus we expect that Eq. 4 also applies to nanocomposites as verified next in this section. In addition, we propose that the depth of the nano surface layer δ_c, is proportional to the pyrolysed depth δ_{pyro} (i.e. the depth of the material pyrolysed) and this proposition will be verified in the numerical result.

Now a new parameter can be defined for nanocomposites to characterise the reduction of the heat flux on the unpyrolysed material. This parameter (hereafter denoted by $ratio_{flux}$) can be expressed in Eq. 5, as the ratio of the net incoming heat flux on the surface for the case when there is no surface ($\dot{q}''_{net\_0}$) over the actual heat flux at the interface of the surface (nano) layer and virgin material in the presence of the surface layer ($\dot{q}''_{net}(t)$).

$$ratio_{flux}(t) = \frac{\dot{q}''_{net\_0}}{\dot{q}''_{net}(t)} \tag{5}$$

By definition, $ratio_{flux}$ has a value of one prior to formation of the surface layer, and increases as the fire retardancy of surface layer increases (e.g. the depth of the surface layer increases). The expressions of $\dot{q}''_{net\_0}$ and $\dot{q}''_{net}(t)$ will be derived next.

The net incoming heat flux on a pyrolysing surface for the case when there is no surface layer, $\dot{q}''_{net\_0}$, can be calculated using the energy balance on the surface with the surface temperature being the ignition temperature as shown in Figure 27:

$$\dot{q}''_{net\_0} = \dot{q}''_{cone} + \dot{q}''_{flame} - \sigma T_{ig}^{\ 4} - h_c(T_{ig} - T_{amb}) \tag{6}$$

where $\dot{q}''_{cone}$ is the nominal heat flux from the cone, $\dot{q}''_{flame}$ represents a sudden increase of the imposed heat flux after ignition due to the flame and a constant value of 10 kW/m^2 is used following [19], T_{ig} denotes the ignition temperature that is determined from the ignition tests, σ is the Stefan-Boltzmann constant, the convective heat transfer coefficient h_c takes a value of 7 kW/m-K based on the finding in a previous study using a steel plate in the cone calorimeter [20], and the ambient temperature T_{amb} = 300K.The radiation from the ambient is negligible whereas the absorption coefficient α and the emissivity ε shown in Fig. 27 are taken equal to one. Note that for a given material exposed to a constant heat flux $\dot{q}''_{net\_0}$ remains constant during pyrolysis.

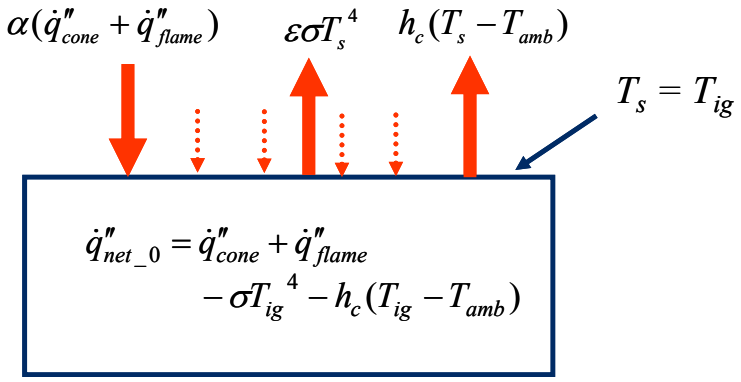

Figure 27. Schematic view of heat transfer for the case when there is no surface layer.

A schematic view of heat transfer during pyrolysis of nanocomposite with the surface layer is shown in Figure 28. We note that similar to charring materials the temperature at the interface of surface layer and virgin material is assumed to be at the ignition temperature whilst the surface temperature may increase far beyond the ignition temperature. The increased surface temperature has the primary effect on the reduced heat flux transfer to the virgin layer because of the increasing re-radiation heat losses. However, because the surface temperature is unknown, the actual heat flux at

the interface can not be derived based on the energy balance of the surface layer, but fortunately it can be determined by considering the energy balance of the unpyrolysed (virgin) layer based on the experimental mass loss data with the assistance of numerical calculations as following.

We consider here the 1D conduction equation governing the unpyrolysed layer:

$$\rho c \frac{\partial T}{\partial t} = \frac{\partial}{\partial x}\left(k \frac{\partial T}{\partial x} \right) \tag{7}$$

where k, ρ, c are respectively the conductivity, density and specific heat of the polymer, T temperature, t time and x the distance from the surface towards inside the solid. For ease of numerical solutions, $x = 0$ is always located at the top surface as shown in Figure 28. The thickness of the unpyrolysed material also changes as pyrolysis continues. The effective thermal properties (k and c) of the polymer are deduced from the ignition tests as detailed in Section 6.3.

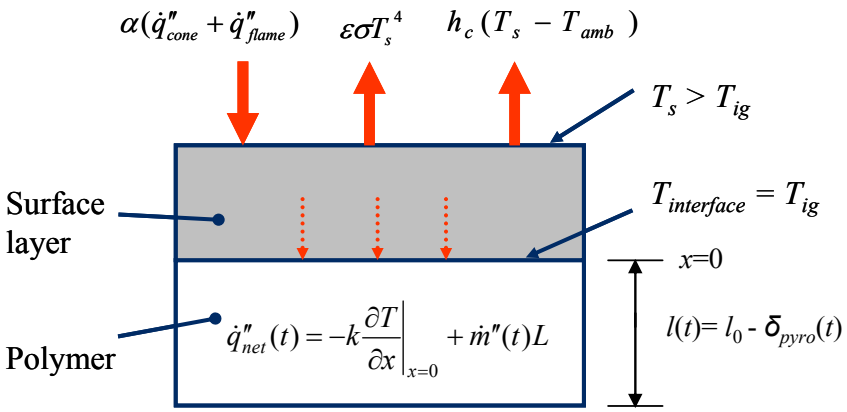

Figure 28. Schematic view of heat transfer during pyrolysis of nanocomposite with the surface layer.

The boundary conditions for the front ($x = 0$) and back ($x = l(t)$) surfaces are respectively:

Before ignition:

$$-k\frac{\partial T}{\partial x}\Big|_{x=0} = \alpha\dot{q}''_{cone} - \varepsilon\sigma T_s^4 - h_c(T_s - T_{amb})$$
$$-k\frac{\partial T}{\partial x}\Big|_{x=l} = 0 \tag{8}$$

After ignition:

$$T_s = T_{ig}$$
$$-k\frac{\partial T}{\partial x}\Big|_{x=l(t)} = 0 \tag{9}$$

where the backside is designed to be adiabatic as the samples were insulated at the back with low conductivity Cotronic ceramic paper. The surface emissivity ε and the surface absorptivity α are assumed to be one as the exposed top surface of the samples in the experiments was painted with black paint. After ignition the sample thickness, $l(t)$, decreases with time due to mass loss and is

therefore calculated dynamically by subtracting the pyrolysed depth, δ_{pyro}, from the initial thickness, where δ_{pyro} is obtained by integrating the instantaneous experimental mass loss rate, $\dot{m}''$, as:

$$\delta_{pyro} = \frac{\int_0^t \dot{m}''(\tau) d\tau}{\rho} \tag{10}$$

Whilst solving Eq. 2, one can construct numerically the conduction heat flux on the surface of the unpyrolysed material (i.e. $-k\partial T/\partial x\big|_{x=0}$) and thus the actual heat flux transferred into the unpyrolysed material can be found by considering the energy balance at the surface of the unpyrolysed material as shown in Figure 28:

$$\dot{q}''_{net}(t) = -k\frac{\partial T}{\partial x}\bigg|_{x=0} + \dot{m}''(t)L \tag{11}$$

where $\dot{m}''(t)$ is the experimental mass loss rate, L is the latent heat of pyrolysis, which can be determined from DSC tests or by considering the energy balance at the peak mass loss rate in the cone calorimeter tests. Because of the difficulties in accurately measuring the heat of pyrolysis in DSC, manifested by the fact that the measurements at University of Ulster are only about half the values in another study in [8]., the values determined in the cone calorimeter, which are also close to those reported in [8], are used in the present analysis.

6.2 Numerical details

Equation 7 was discretised in space using the finite volume method and in time the fully implicit method to ensure numerical stability. The discretised equation was solved using a tri-diagonal matrix algorithm (TDMA) solver. A non-uniform grid system was used, with denser grids towards the pyrolysis front where large temperature gradients are expected. The smallest grid size is about 0.01mm. Sensitivity tests showed that for 6mm samples a grid number of 48 and a timestep of 0.05s yield results which are essentially independent of the grid size and timestep. As the sample thickness l changes with time due to mass loss, the mesh was regenerated at each new timestep, and the temperatures at the grid nodes on the new mesh were determined from the ones on the old mesh using a linear interpolation.

6.3 Deduced effective thermal properties for the PA6 nanocomposite

For the thermally thick condition, effective thermal properties (i.e., thermal inertia, $k\rho c$, and ignition temperature, T_{ig}) can be deduced from time to ignition experiments which follow a standard procedure in the cone calorimeter. Theory and experiments showed that ignition usually occurs at a constant temperature independent of the imposed heat flux. The effective thermal properties can thus be determined at a time which is inversely proportional to the square root of the external heat flux. However, if materials are thermally intermediate (i.e. neither thermally thick nor thermally thin) a modification of plotting ignition time data is required in order to obtain thermal properties and the critical heat flux [21]. The corrected ignition time for the PA6 nanocomposite is plotted in Figure 29, where F_1 and F_2 are given in [21] as functions of $X = \delta/(\alpha_2 \cdot \dot{q}''_{cone})$ and have a value of one for the thermally thick condition.

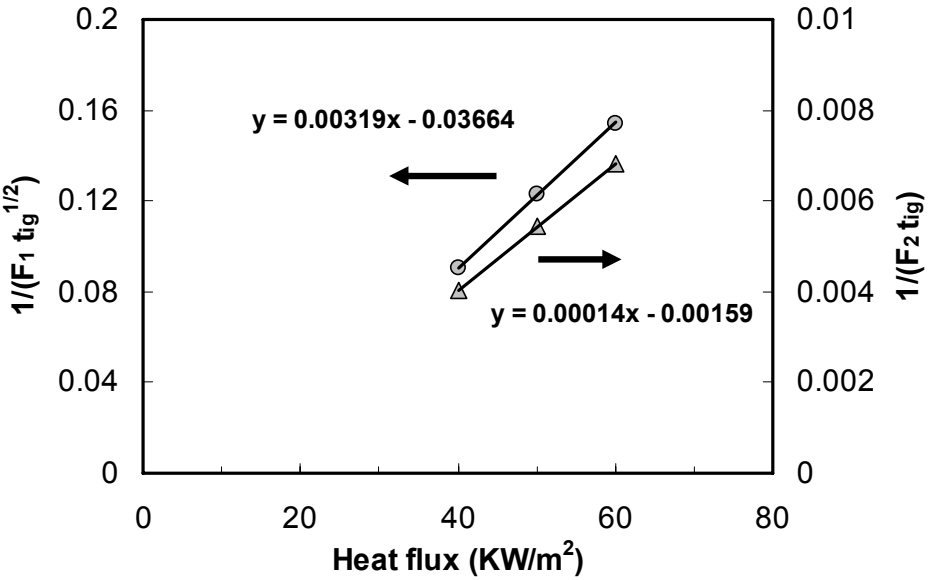

Figure 29. Corrected ignition time for the PA6 nanocomposite. Thermal diffusivity, α_2 ,equals to 0.9×10^{-7} m^2/s. F_1 and F_2 are derived analytically in [13] as functions of $X = \delta/(\alpha_2 \cdot \dot{q}''_{cone})$, where δ is the initial sample thickness and $\dot{q}''_{cone}$ is the nominal heat flux from the cone.

The diffusivity, α_2, is subsequently determined under the condition that the intercepts of the linear fits for the thermally thick and thin conditions are equal. For the PA6 nanocomposite, when the diffusivity is equal to 0.9×10^{-7} m^2/s, the intercepts are almost the same at about 11.5 kW/m^2. These intercepts are equal to the 0.64 fraction of the critical heat flux (below which there is no ignition) for ignition [21], and thus the critical heat flux can be calculated equal to 11.5/0.64 = 17.9 kW/m^2. The ignition temperature can then be calculated by considering the critical heat flux equal to surface re-radiation and convection losses:

$$\dot{q}''_{cri} = \sigma\left(T_{ig}{}^4 - T_{amb}{}^4\right) + h_c\left(T_{ig} - T_{amb}\right) \tag{12}$$

To determine the thermal inertia, we note that that the ignition time for thermally thick materials can also be expressed as:

$$t_{ig} = \frac{\pi}{4} k\rho c \frac{\left(T_{ig} - T_{amb}\right)^2}{\left(\dot{q}''_{cone} - 0.64\dot{q}''_{cr}\right)^2} \tag{13}$$

From the slope of the plot for the thermal thick condition in Figure 29, the thermal inertia $k\rho c$ can be found using Eq. 13 having a value of 0.62 kJ^2/m^4-K^2-s. With density and diffusivity known, the specific heat and conductivity can then be derived. A summary of the thermal properties and critical heat flux is presented in Table 5. For comparison purpose, the data reported in [22] for pure PA6 at the ambient temperature are also included. There is in general good consistency between the two sets of data. The fact that the deduced specific heat in this work is higher than the one reported in [22] can be explained by the dependence of the specific heat on temperature as noted by our DSC measurements showing that the specific heat increases from 1600 to 3000 J/kg-K when temperature changes from ambient to around 490K.

Table 5. Effective thermal properties of the PA6 nanocomposite derived from the ignition tests, along with the literature values reported for pure PA6 in [22].

	α m^2/s	$\dot{q}''_{cri}$ kW/m^2	T_{ig} K	k W/m-K	c J/kg-K	$k\rho c$ kJ^2/m^4-K^2-s	L J/g
PA6/NC(UBE)	0.9×10^{-7}	17.9	725	0.23	2300	0.62	-
PA6 [22]	1.37×10^{-7}	-	705	0.24	1550	-	1000

For the latent heat of pyrolysis, it is worthwhile to note that a wide range of values measured using DSC were reported by in the literature. For example, in [8], a value of 1390±90 J/g was reported for PA6, whereas 560 J/g was reported by Frederick & Mentzer [23]. In addition, the DSC tests by our group showed the average value for PA6 is around 500 J/g. The disagreement highlights the large uncertainties in measuring the heat of pyrolysis. As discussed earlier, an alternative method is to examine the energy balance at the second peak MLR/HRR in the cone for pure polymers. At the second peak MLR/HRR the sample has a uniform temperature and thus the internal conduction can be neglected. After examining the data obtained at different heat fluxes, an average value of 100 J/g was found. In the present study, we made the assumption that the PA6 nanocomposite has the same heat of pyrolysis as pure PA6, because the small amount of nanoparticles was used and DSC and TGA data also showed little different between the nanocomposite and pure PA6. This assumption is also justified by the fact that pure polymers and polymer nanocomposites have the same effective heat of combustion from the cone calorimeter results indicating again that there is no chemical effect by nanoparticles.

6.4 Results and discussions

The key calculation results in the heat flux ratio, $ratio_{flux}(t) = \dot{q}''_{net\_0} / \dot{q}''_{net}(t)$, which could be expressed as a function of time. But in order to examine the validity of Eq. 4 for nanocomposites, the heat flux ratio is presented as a function of the pyrolysed depth, i.e., the thickness of the pyrolysed depth.

Derived correlation between the heat flux ratio and the pyrolysed depth

The reduction of the external heat flux to the sample due to a surface layer formation, as $ratio_{flux}(t) = \dot{q}''_{net\_0} / \dot{q}''_{net}(t)$, is plotted in Figure 30 against the pyrolysed depth, δ_{pyro}, for one of the duplicated tests at $40kW/m^2$ (6mm sample). Three regions can be identified, namely a) a relatively constant $ratio_{flux}$ in the first region, b) a nearly linear increase in the second region and 3) a sharp increase in the third region. In the first region, the relatively constant heat flux ratio indicates that nanoparticles are less effective at this stage of pyrolysis because the depth of the surface layer is small. Its value (about 1.15) is slightly higher than the ideal value (one), which could be due to the assumption in the calculations of a sudden increase of the imposed heat flux after ignition to represent the flame effect. The sudden increase in the third region is due to the fact that the mass loss rate and the conduction heat flux term (the first term on the RHS of Eq. 11) are small at the end of pyrolysis resulting in small values of $\dot{q}''_{net}$ and thus large values of $ratio_{flux}$. It is however the second region representing the main pyrolysis process that is of the most importance in the present analysis. This region is characterised by a nearly linear increase of $ratio_{flux}$ against δ_{pyro}.

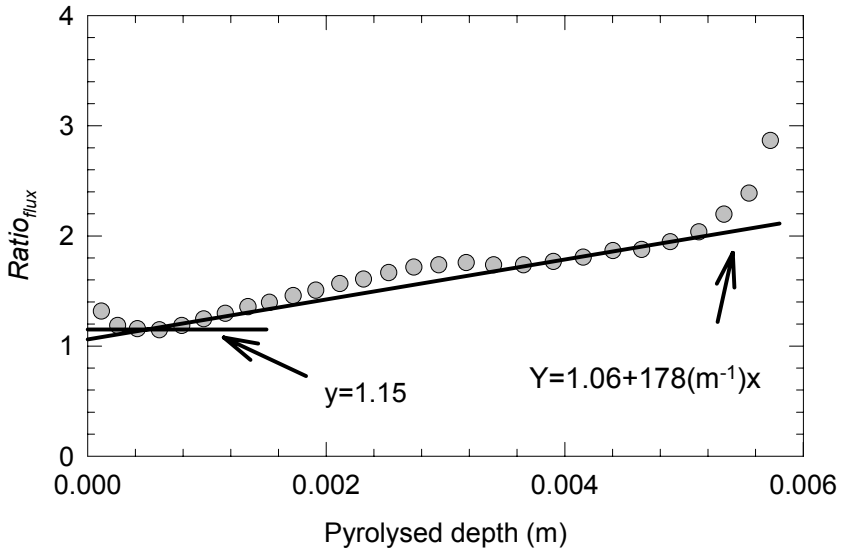

Figure 30. Calculated instantaneous heat flux ratio, $ratio_{flux}(t) = \dot{q}''_{net\_0} / \dot{q}''_{net}(t)$, against the pyrolysed depth, δ_{pyro}, for one of the duplicated tests at 40kW/m^2 (the sample thickness is 6mm). Two lines represent the best fits of the calculated results.

The finding shown in Figure 30 verifies our early proposition that the thickness of the surface layer is proportional to the pyrolysed depth. The thickness of the surface layer is assumed to be proportional to the amount of nanoparticles accumulated on the surface assuming that nanoparticles initially are uniformly distributed in the polymer and nanoparticles do not pyrolyse during burning (dehydroxylation of nanoparticles occurs upon heating but the total weight loss is only about 6 % of the nanoparticles weight and thus negligible). The assumption of uniform distribution of nanoparticles in the PA6 nanocomposite is also supported by our results of Scanning Electron Microscopy (SEM), X-ray diffraction (XRD), Rheological analyses and Nuclear Magnetic Resonance (NMR) spectroscopy measurements, indicating that the PA6 nanocomposite used in this study is fully exfoliated [1,2]. By best fitting in Figure 30, one obtains the following approximate correlation:

$$ratio_{flux} = 1.15 \quad for \quad \delta_{pyro} < 5\times10^{-4} m \tag{14a}$$

$$ratio_{flux} = 178(m^{-1})\delta_{pyro} + 1.06 \quad for \quad \delta_{pyro} >= 5\times10^{-4} m \tag{14b}$$

Here the third region is ignored anticipating it has negligible influence on the main pyrolysis process because it is relatively short.

Predicted mass loss rates

In this section, the correlation in the heat flux ratio versus the pyrolysed depth given by Eq. 14 is incorporated into the numerical model to predict the pyrolysis process of the PA6 nanocomposite at different heat fluxes and thicknesses. The boundary conditions remain as those given by Eqs. 8 and 9. However, the MLR is now calculated from the heat flux ratio correlation in Eq. 14 as,

$$\dot{m}''(t) = \frac{\dot{q}''_{cone} + \dot{q}''_{flame} - \sigma T_{ig}{}^4}{ratio_{flux} \cdot L} \tag{15}$$

where $ratio_{flux}(t)$ is dynamically determined from $\delta_{pyro}(t)$ using Eq. 14 and δ_{pyro} is obtained by integrating the calculated instantaneous MLR in time using Eq. 10.
Figure 31 compares the predicted MLRs with the experimental ones for the 6mm sample at different heat fluxes. The predictions generally capture the trends of the experimental data and are in quantitative agreement with the measurements. This is an important finding of this work as the correlation in the heat flux ratio and pyrolysed depth (Eq. 14) was deduced for one heat flux ($40kW/m^2$) but our results demonstrate that the same correlation can also be applied to predict pyrolysis at other heat fluxes. In other words the correlation is independent of the heat flux but depends only on the depth of pyrolysed material, or equivalently the amount of nanoparticles accumulating on the surface. As we have adopted a simple correlation between $ratio_{flux}$ and δ_{pyro}, some discrepancies are noted at the end of the pyrolysis process, where the predictions fail to reproduce the drops of the experimental MLRs. This is, however, consistent with the treatment that the region corresponding to the end of the pyrolysis in Figure 30 was ignored.

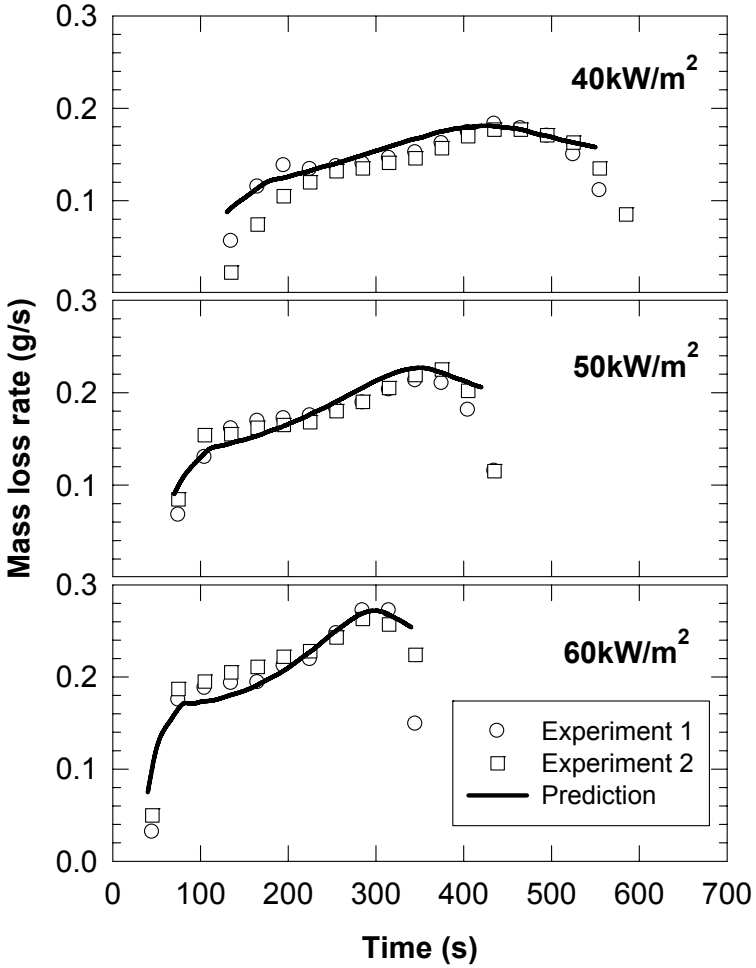

Figure 31. PA6 nanocomposite – comparisons of experimental and predicted MLRs for 6mm samples at three heat fluxes.

To examine the validity of the present methodology to samples of different thicknesses, the same correlation given by Eq. 14 is used to predict the burning rate for the 12 and 24 mm samples at $50kW/m^2$. For the calculation of the thicker samples the same parameters were used except that 64 grids were used for the 12mm sample and 96 grids for the 24mm sample. A comparison of the predicted and experimental mass loss rates is shown in Figure 32. First we note that there are some unexpected dips and peaks in the experimental results because the thicker samples were obtained by gluing of 6mm sample (especially clear for the 24mm sample). Apparently the contact between different layers of the samples affects heat transfer mechanisms and thus the pyrolysis process. Nonetheless the overall results are encouraging as the predictions reproduce the typical behaviours

of charring materials with two peaks that also agree quantitatively with the experimental data. The average relative differences between the predictions and measurements are within 20%. For the 12mm sample the model seems to underestimate slightly the MLR under 600s, after which the agreement between the prediction and experiment is reasonably good, whereas for the 24mm sample the model generally underpredicts the MLR; however the experimental errors (fluctuations) are clear for this thickness preventing from further quantitative assessment of the accuracy of the model.

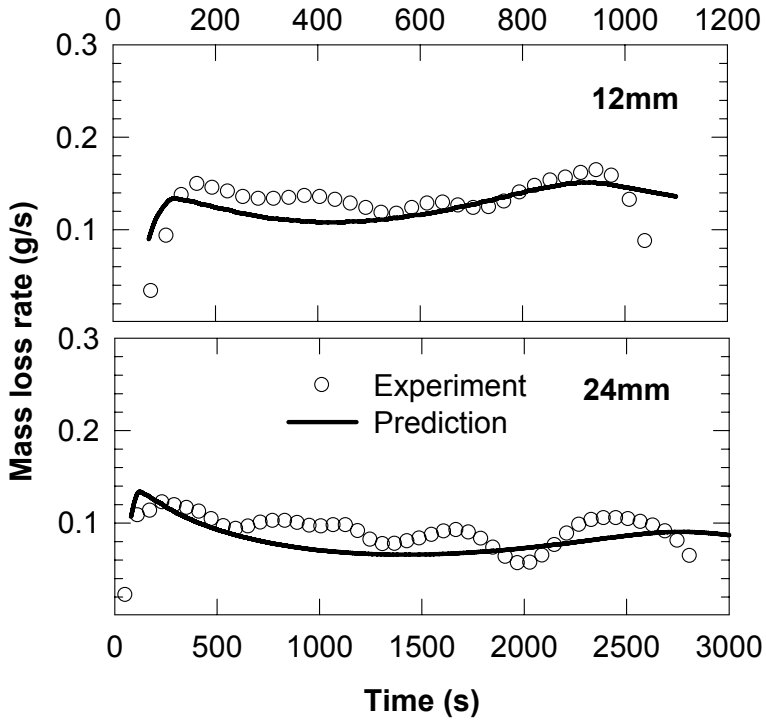

Figure 32. PA6 nanocomposite – comparisons of experimental and predicted MLRs for 12 and 24 mm samples at 50kW/m^2.

7. Further validation of the model

7.1 Application to EVA and PBT nanocomposites

7.1.1 Material and experimental details

In this work, tests were also conducted for other polymers with different type and/or loading of nanoparticles. These materials are an ethylene-vinyl acetate (EVA) nanocomposite with 5 wt. % organoclay by Kabelwerk EUPEN AG / Belgium, and a polybutylene terephthalate (PBT) nanocomposite with 5 wt. % Sepiolite. The samples size is the same as the one for PA6 (i.e., 100×100×6 mm). Similar to the PA6 tests, three external heat fluxes (40, 50 and 60 kW/m^2) were used with duplicated tests at each heat flux level.

7.1.2 Experimental ignition times

The duplicated tests, in general, show good repeatability, and the average ignition times of the duplicated tests for the EVA and PBT nanocomposites are summarised in Table 6.

Table 6. Average experimental ignition times (in seconds) for EVA and PBT nanocomposites at different heat fluxes.

	40kW/m^2	50kW/m^2	60kW/m^2
EVA nanocomposite	70	47.5	28
PBT nanocomposite	73	39.5	27.5

7.1.3 Deduced effective thermal properties

The methodology [21] that has been used to the PA6 nanocomposite to deduce the thermal properties and critical heat flux was applied to the EVA and PBT nanocomposites (section 7.1.1). The corrected ignition times as a function of the external heat flux for both EVA and PBT nanocomposites are shown in Figure 33. The final deduced thermal properties and critical heat flux are summarised in Table 7, along with the values reported for pure EVA and PBT in [22].

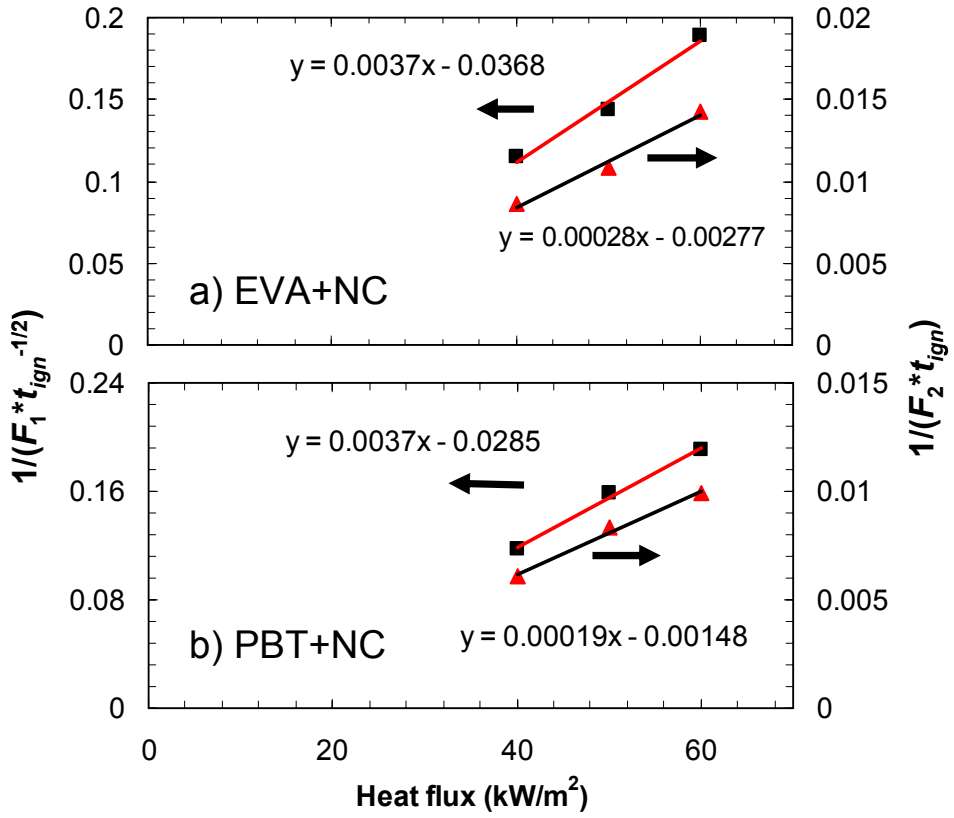

Figure 33. Corrected ignition time for a) EVA and b) PBT nanocomposites. Thermal diffusivity, α ,equals to 2.6×10^{-7} and 1.25×10^{-7} m^2/s for EVA and PBT nanocomposites respectively.

Table 7. Effective thermal properties of PA6, EVA and PBT nanocomposites derived in this work, together with those reported for pure polymers in [22].

	α m^2/s	$\dot{q}''_{cri}$ kW/m^2	T_{ig} K	k W/m-K	c J/kg-K	$k\rho c$ kJ^2/m^4-K^2-s	L J/g
PA6/NC	0.9×10^{-7}	17.9	725	0.23	2300	0.62	1000-

PA6 [22]	1.37×10^{-7}	-	705	0.24	1550	-	
EVA/NC	2.6×10^{-7}	11.3	668	0.44	1845	0.765	2000
EVA [22]	2.67×10^{-7}	-	-	0.34	1370	-	
PBT/NC	1.25×10^{-7}	12.1	680	0.28	1733	0.645	1000
PBT [22]	1.01×10^{-7}	-	650	0.22	1610	-	

7.1.4 Results and discussions

In Figure 34a, the history of the calculated heat flux ratio, $ratio_{flux}$, is plotted against the pyrolysed depth, δ_{pyro}, for the EVA nanocomposite for one of the duplicated tests at 50kW/m^2. As we noted previously for the PA6 nanocomposite, the heat flux ratio $ratio_{flux}$ increases linearly with δ_{pyro} during the main pyrolysis process. These results further support the validity of the Eq. 4 for nanocomposites. By neglecting the region near the end of pyrolysis and drawing two lines of best fit in Figure 34a, we obtain:

$$ratio_{flux} = 1.2 \text{ for } \delta_{pyro} < 4\times10^{-4} m \quad (16a)$$

$$ratio_{flux} = 500(m^{-1})\delta_{pyro} + 1.0 \text{ for } \delta_{pyro} >= 4\times10^{-4} m \quad (16b)$$

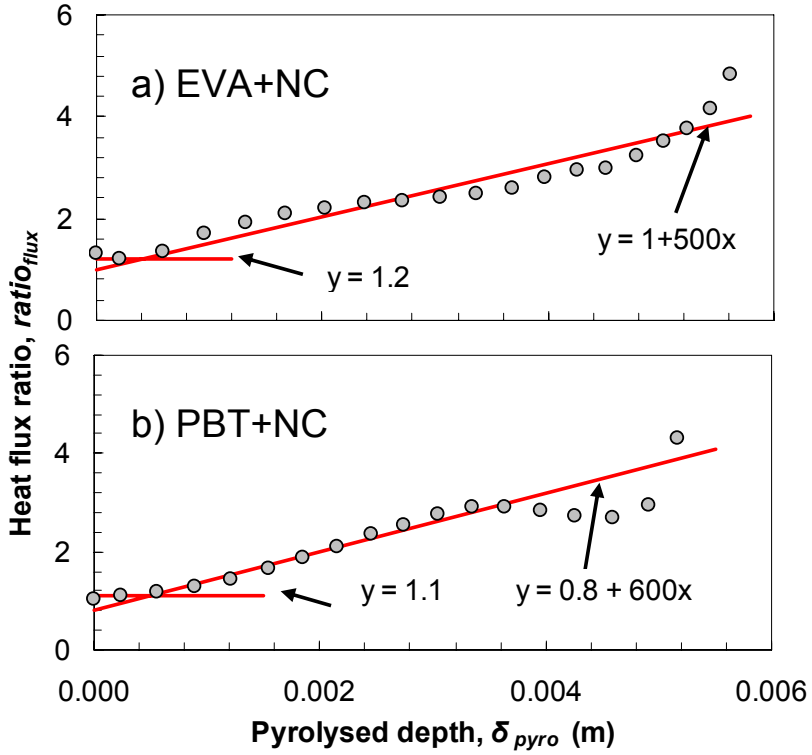

Figure 34. Calculated heat flux ratio, ratioflux, against pyrolysed depth, δpyro, for a) EVA and b) PBT nanocomposites at 50kW/m2. Two lines represent the best fits of the calculation results, which are also used to predict the mass loss rate.

Figure 34b shows the calculated $ratio_{flux}$ against δ_{pyro} for the PBT nanocomposite at 50kW/m^2. Similar to the result of the EVA nanocomposite, $ratio_{flux}$ increases linearly with δ_{pyro}, but only up to about 4mm. The further decrease of $ratio_{flux}$ with δ_{pyro} is consistent with the observation in the experimental data where slightly increases of the MLR were noted. The different behaviour of the

PBT nanocomposite from the EVA nanocomposite or from the PA6 nanocomposite indicates that the effect of the surface (nano) layer depends on the type of polymers as well as on the type and loading of nanofillers. Nonetheless, through best fitting we obtain:

$$ratio_{flux} = 1.1 \text{ for } \delta_{pyro} < 5\times10^{-4} m \quad (17a)$$

$$ratio_{flux} = 800(m^{-1})\delta_{pyro} + 0.8 \text{ for } \delta_{pyro} >= 5\times10^{-4} m \quad (17b)$$

The correlation given by Eqs. 16 and 17 are used to predict the MLRs at various heat flux, and the results are given in Figures 35 and 36 for the EVA and PBT nanocomposites respectively. In general, the predictions are in good agreement with the measurements. The ignition times (indicated by sudden increases of the MLRs) and the first peak MLRs are correctly predicted. These results again demonstrate that the same correlations can also be applied to predict pyrolysis at other heat fluxes. In other words, for a given nanocomposite the proportional factor (between the heat flux ratio and pyrolysed depth) is independent of the heat flux and, as shown for the PA6 nanocomposite, of the initial sample thickness, but depends only on the amount of nanoparticles accumulating on the surface or equivalently the pyrolysed depth.

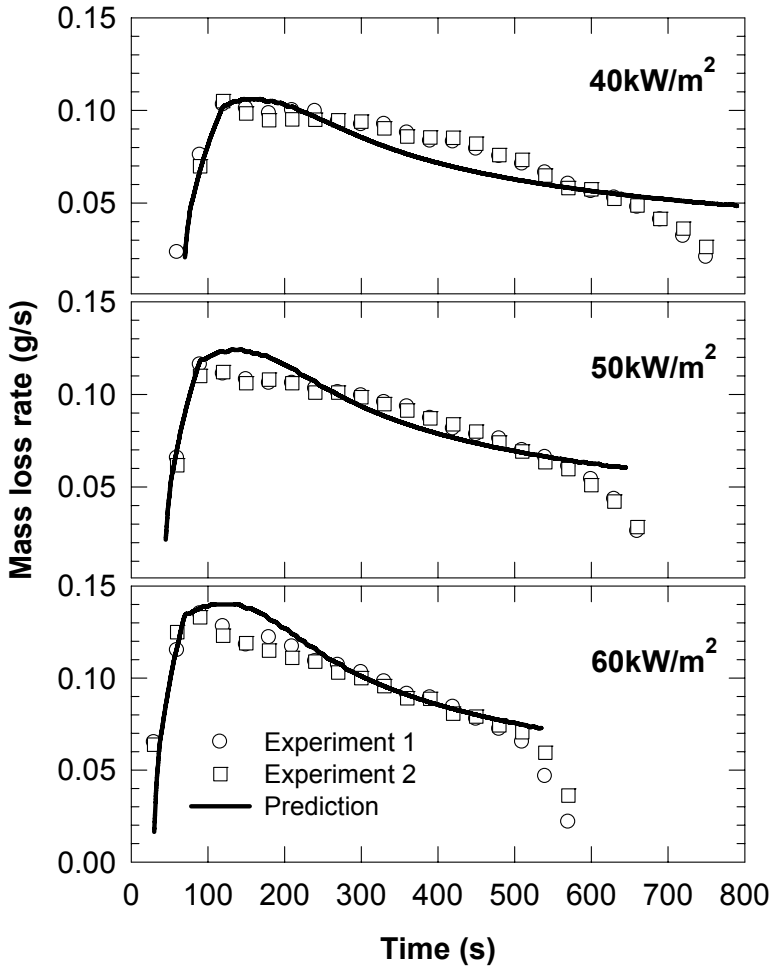

Figure 35. EVA nanocomposite – comparisons of experimental and predicted MLRs for 6mm samples at three heat fluxes.

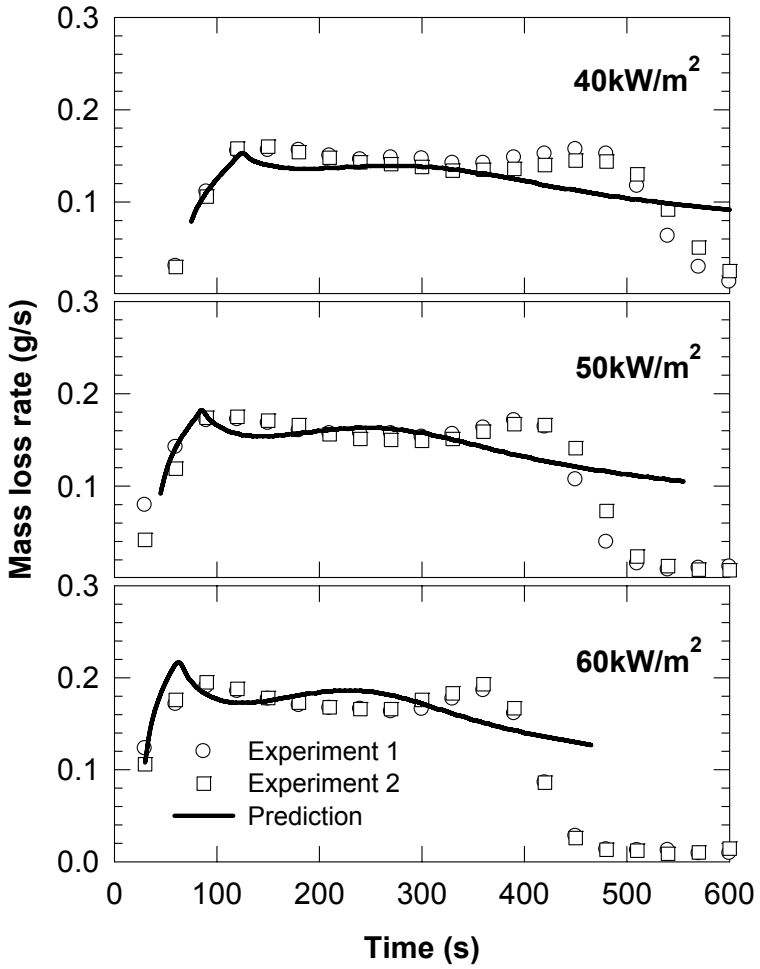

Figure 36. PBT nanocomposite – comparisons of experimental and predicted MLRs for 6mm samples at three heat fluxes.

7.2 Extension of the model for different loadings of nanoclay

To examine the optimised loading for a PA6/MMT nanocomposite, a series of tests were conducted in the cone calorimeter [24] with various (2, 5 and 10%) loadings of nanofillers. The experimental HRR/MLR are reproduced in Figure 37, where it was found that the HRR/MLR decrease as the concentration of nanofillers increase up to 10%. The main objective of this section is to extend the model to account for the change in the nanofiller loading, or, in other words, to use the experimental data at one nanofiller loading to predict the burning behaviours of nanocomposite at other loadings.

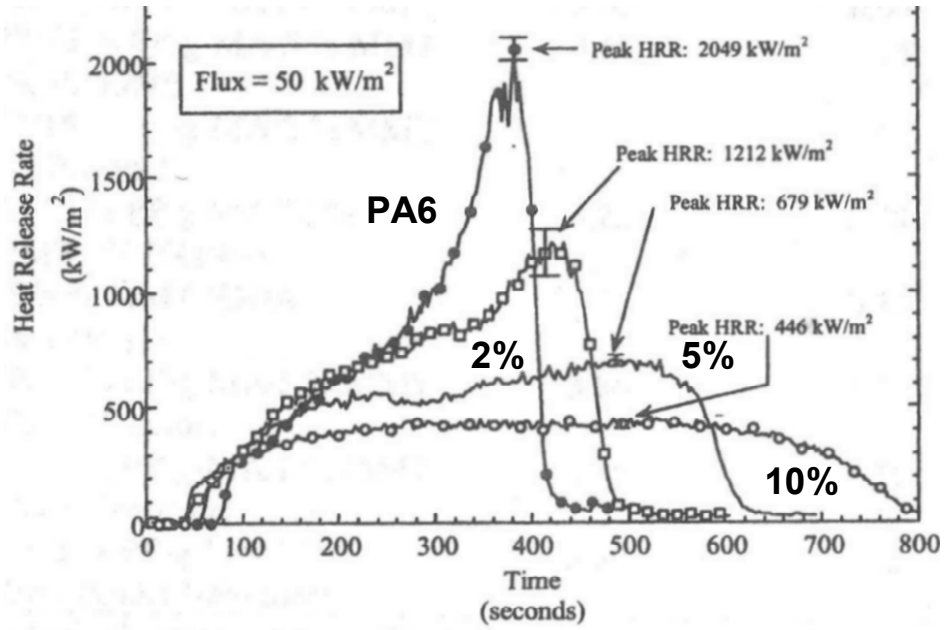

Figure 37. HRRs for pure PA6 and intercalated PA6/MMT nanocomposites (mass fraction 2%, 5%, and 10%). Reproduced from [24].

As shown earlier, for a given nanocomposite (PA6, EVA, and PBT) the heat flux ratio is proportional to the pyrolysed depth by a factor K, although that the factor K may vary with the type of polymer and the type and loading of nanofillers. Furthermore, we assume implicitly that the density and conductivity of the surface layer do not change with different nanofiller loadings, thus the factor K would be proportional to the loading. With this assumption, the factor K for one of the three loadings is found by optimisation or, more specifically, comparing the predictions with the experimental data, whereas that for other loadings can be determined proportionally. For example, for the 5% case K is found to be 142 (m^{-1}). Thus, we have:

$$ratio_{flux} = 1.15 \text{ for } \delta_{pyro} < 5\times10^{-4} m \quad (18a)$$

$$ratio_{flux} = 142(m^{-1})(\delta_{pyro} - 5\times10^{-4})\times C_{nano}/5 + 1.15 \text{ for } \delta_{pyro} >= 5\times10^{-4} m \quad (18b)$$

where C_{nano} denotes the nanofiller loading (%).

Figure 38 shows a comparison of the predicted and experimental MLRs at different nanofiller loadings. It is worthwhile to point out that the experimental MLRs for 2 and 10 % nanocomposites were not reported, but calculated by dividing the HRRs in Figure 37 over the effective heat of combustion (EHC). The EHC was determined from the HRR and MLR of 5% nanocomposite, having a value of 33±3 kJ/kg. The error bars in Figure 38 thus indicate uncertainties of ±10 %. It is noted that the model predicts that the MLR increases with increasing concentration of nanofillers. The prediction for the 10% case is good, whereas the model underestimates the MLR for the 2% case. This underestimation may be explained partly by the observation that the experimental HRR for the 2% case is essentially the same as pure PA6 up to 280s [24], indicating that no surface layer was formed during this period because of the small amount of nanofillers and the PA6 nanocomposite being intercalated. In addition, the assumption that the pyrolysed depth is proportional to the nanofiller loading is only approximate implying that the packing density of the nanofiller and the conductivity of the surface layer may change slightly with the nanofiller loading.

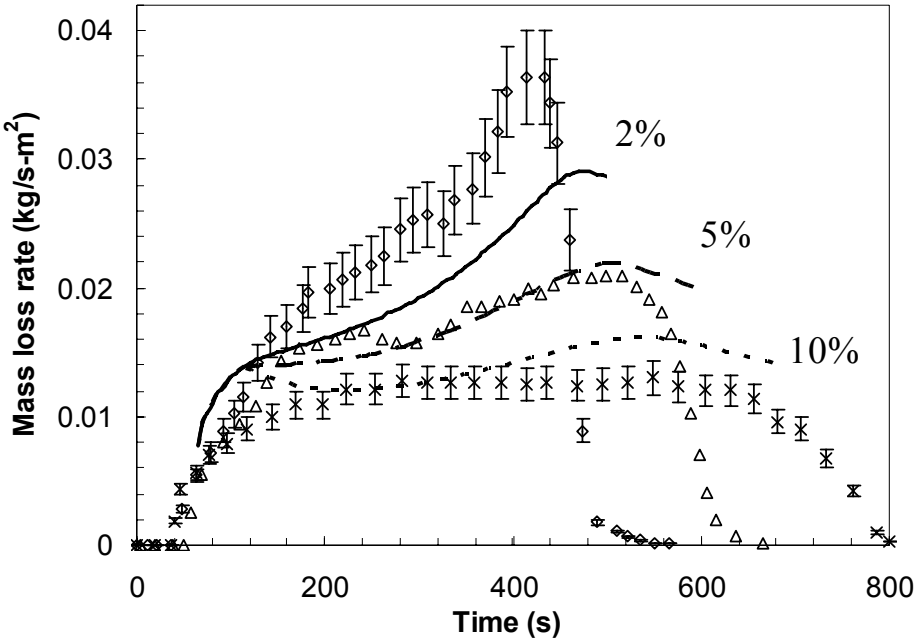

Figure 38. Comparisons of the predicted and experimental MLRs for different nanofiller loadings at 50kW/m2. The MLRs for 2 and 10 % cases are calculated from the reported HRRs for these cases and the effective heat of combustion (EHC) determined from the HRR and MLR data for the 5% case.

8. Conclusions

We have shown in this paper that microscale measurements can provide a good screening method for the design of fire resistant materials modified by nanoparticles (and fire retardants) and also, they can be used to quantitatively model and predict the behaviour in mesoscale experiments even though an additional parameter is needed to predict the reduced mass loss rate in the mesoscale experiments. The major breakthroughs and challenges are the following:

1. Rheometry of the nanocomposite polymer provides information about the viscosity and shear modulus that can be used to predict the melting behaviour in mesoscale experiments.
2. Rheometry can also point to the consistency and strength of the char layer.
3. TGA/ATR for the structure of the condensed phase at different temperatures can also provide information about the strength and consistency of the char.
4. DCS/MDSC can be used to determine the thermal and transport properties as well as the heat of melting and pyrolysis. The measurement of heat of pyrolysis is very challenging and needs more investigation.
5. TGA/ FTIR provides the composition of the pyrolysing gases but it needs simplifications in the calibration concerning the quantification of the product yields . These results are consistent with the tube furnace and cone results but more work is needed in this area.
6. The tube furnace is a practical method for assessing the production of toxic gases but it needs more work to make the results applicable for modelling large scale fires.
7. A methodology and a new parameter has been developed to quantify the effect of the nanoparticles in reducing the mass loss rate in the mesoscale experiments (i.e. cone) where all other properties have been determined from the microscale experiments

Acknowledgements

We thank all partners in the PREDFIRE project, Jeff Gilman for useful discussions and Charlie Wilkie for inviting us to prepare this review. Finally, we thank Mary Delichatsios for a useful review of the final document.

References

[1]. Samyn, F. Bourbigot, S. Jama, C. Bellayer, S. Nazare, S. Hull, R. Castrovinci, A. Camino, G., European Polymer Journal, 44 (6), p.1631-1641
[2]. Samyn, F. Bourbigot, S. Jama, C. Bellayer, S. Nazare, S. Hull, R. Castrovinci, A. Camino, G. , European Polymer Journal, 44 (6), p.1642-1653.
[3]. Ohlemiller, T. J.; Shields, J. R. , Aspects of the Fire Behavior of Thermoplastic Materials., NIST TN 1493; NIST Technical Note 1493; 158 p. January 2008.
[4]. Ohlemiller, T. J.; Shields, J. R. , Assessment of a Medium-Scale Polyurethane Foam Flammability Test. NIST TN 1495; NIST Technical Note 1495; 45 p. February 2008.
[5]. Cipiriano, B. H.; Kashiwagi, T.; Raghavan, S. R.; Yang, Y.; Grulke, E. A.; Yamamoto, K.; Shields, J. R.; Douglas, J. F., Effects of Aspect Ratio of MWNT on the Flammability Properties of Polymer Nanocomposites. Polymer, Vol. 48, No. 1620, 6086-6096.
[6]. Kashiwagi, T. , Flame Retardant Mechanism of the Nanotubes-Based Nanocomposites. Final Report. NIST GCR 07-912; Final Report; 68 p. September 2007.
[7]. Kashiwagi, T.; Fagan, J.; Douglas, J. R.; Yamamoto, K.; Heckert, A. N.; Leigh, S. D.; Obrzut, J.; Du, F.; Lin-Gibson, S.; Mu, M.; Winey, K. I.; Haggenmueller, R., Relationship Between Dispersion Metric and Properties of PMMA/SWNT Nanocomposites. Polymer, Vol. 48, No. 16, 4855-4866.
[8]. S.I. Stoliarov, R.N. Walters, Polymer Degradation and Stability 93 (2008) 422-427
[9]. Pramoda, K.P, Liu, T., Liu, Z., He, C., Sue, H, J. (2003) "Thermal degradation behaviour of polyamide 6/ clay nanocomposites" Polymer Degradation and Stability, pp. 47-56.
[10]. Jang, B.N. and Wilkie, C. A. (2005) The effect of clay on the thermal degradation of polyamide 6 in polyamide 6/clay nanocomposites. Polymer pp. 3264-3274
[11]. M. Herrera, G. Matuschek, A. Kettrup, Chemosphere, 2001, 42, 601-607
[12]. Bourbigot S, Le Bras M, Dabrowski F, Gilman JW, Kashiwagi T. (2000) PA6-Clay Nanocomposite Hybrid as Char Forming Agent in Intumescent Formulations, Fire and Materials, 24, pp. 201-208.
[13]. Stec, A.A.; Hull, T.R.; New Strategies and Mechanisms, Royal Society of Chemistry, (In press Mar 2008).
[14]. de Ris, JL, and Khan MM. Sample holder for determining material properties. Fire Mater. 2000;24:219-226.
[15]. Kashiwagia, T., Grulkeb, E., Hildingb, J., Grotha, K., Harrisa, R., Butlera, K., Shieldsa, J., Kharchenkoc, S. and Douglas, J. (2004) Thermal and flammability properties of polypropylene/carbon nanotube nanocomposites, Polymer 45 pp. 4227-4239.
[16]. Staggs, J.E.J. (2005) Savitzky–Golay smoothing and numerical differentiation of cone calorimeter mass data, Fire Safety Journal 40: 493-505.
[17]. Green, J. Phosphorus-containing flame retardants, in Fire Retardancy of Polymeric Materials, Grand, A. F.; Wilkie, C. A.; editors; Marcel Dekker Inc., New York 2000, Chap. 5, pp. 147-170.
[18]. M.A. Delichatsios, J.L. de Ris, An analytical model for the pyrolysis of charring materials, Technical report, J.I. OK0J1.BU, Factory Mutual Research, 1983
[19]. J. Zhang, J. Hereid, M. Hagen, D. Bakirtzis, M.A. Delichatsios, Proceedings of the 5th International Seminar on Fire and Explosion Hazards, 2007, in Press

[20]. M.A. Delichatsios, B. Paroz, A. Bhargava, Fire Saf. J 38 (2003) 219-228
[21]. M.A. Delichatsios, Fire Saf. J. 40 (2005) 197-212
[22]. R.R. Lyon, M.L. Janssens, Polymer flammability. Office of Aviation Research Washington, D.C. 20591, DOT/FAA/AR-05/14, 2005.
[23]. Frederick WJ, Mentzer CC. Determination of heats of volatilization for polymers by differential scanning calorimetry. Journal of Applied Polymer Science 1975;19:1799-1804.
[24]. A.B. Morgan, T. Kashiwagi, R. H. Harris, J.R. Campbell, K. Shibayama, K. Iwasa, J.W. Gilman, Flammability properties of polymer-clay nanocomposites: polyamide-6 and polypropylene clay nanocomposites, American Chemical Society, 2001, pp. 9-23

Appendix B
The material (mesoscale) flammability properties

No	Material	q_{cri}	T_{ig}	$k\rho c$	k	ρ	c	H_c	L [a]	Smoke yield [b]	S	SPH
		kW/m^2	K	kJ^2/m^4-K^2-s	W/m-K	kg/m^3	J/kg-K	kJ/g	J/g	g/g		mm
1	PA6	17.6	715	930	0.370	1130	2200	27	1390±90	0.016	9.00	52.50
2	PA6/NF (UBE)	17.9	720	618	0.235	1140	2300	26	-	0.023	8.67	35.61
3	PA6/NF (Cloisite)	-	-	-	-	-	-	26	-	0.030	8.67	27.34
4	PA6/FR	-	-	-	-	-	-	20	-	0.055	6.67	11.71
5	PA6/NF (Cloisite)/FR	-	-	-	-	-	-	19	-	0.057	6.33	10.81
6	EVA	12.9	690	664	0.400	934	1780	32	-	0.0507	10.67	19.33
7	EVA/NF	15.5	723	511	0.364	969	1447	31	-	0.0856	10.33	11.12
8	EVA/FR (MH)	-	-	-	-	-	-	24	-	0.0291	8.00	25.98
9	EVA/NF/FR (MH)	13.5	698	1010	0.402	1384	1815	26	-	0.0294	8.67	27.62
10	EVA/FR (ATH)	-	-	-	-	-	-	22	-	0.0256	7.33	27.34
11	EVA/NF/FR (ATH)	9.85	645	1503	0.490	1420	2159	23.5	-	0.0178	7.83	41.69
12	PPFF	26.6	827	81	0.230	979	361	27.5	-	0.057	9.17	14.90
13	PPFF/NF	16.7	736	207	0.350	961	611	28	-	0.052	9.33	16.60
14	PPFF/FR	13.5	699	246	0.387	981	647	26.5	-	0.060	8.83	13.68
15	PPFF/NF/FR	10.6	657	436	0.467	981	952	26	-	0.055	8.67	14.82
16	PBT[c]	-	-	-	-	-	-	16	-	0.063	5.33	8.51
17	PBT/NF (Cloisite)	18.8	758	372	0.329	1310	865	18	-	0.062	6.00	9.48
18	PBT/FR	24.4	810	147	0.257	1297	440	12	-	0.110	4.00	3.82
19	PBT/NF (Cloisite) /FR	33	874	85	0.182	1313	355	12.5	-	0.111	4.17	3.91
20	PBT/NF (Sepiolite)	-	-	-	-	-	-	17.5	-	0.059	5.83	9.71
21	PBT/NF (Sepiolite) /FR[c]	-	-	-	-	-	-	16.5	-	0.135	5.50	4.04
22	PP	-	-	-	-	-	-	-	1800±80	-	-	-

[a] Data from (Stoliarov & Walters, 2008)
[b] For fire retardant contating materials (i.e. ATH and MH), water loss was substracted from the total mass loss
[c] Tests were conducted with reduced sample size (7.5x7.5cm)

Nomenclatures

q_{cri}	Critical heat flux
T_{ig}	Ignition temperature
$k\rho c$	Thermal inertia
k	Thermal conductivity
ρ	Density
c	Specific heat
H_c	Heat of combustion,
L	Latent heat of pyrolysis
S	Stoichiometric ratio
SPH	Smoke point height